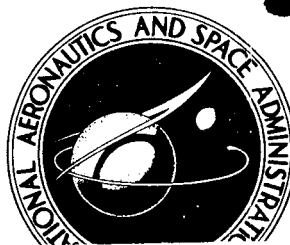


NASA TECHNICAL  
MEMORANDUM



UB  
NASA-TM-X-1402 EN

UB  
NASA TM X-1402

By Authority of 1002-165 Date 4-7-72

FACILITY FORM 602

(ACCESSION NUMBER)	(THRU)
<u>1002-165</u>	<u>2D</u>
(PAGES)	(CODE)
<u>TMX-1402</u>	<u>3</u>
(NASA CR OR TMX OR AD NUMBER)	(CATEGORY)

RADIATIVE HEATING RESULTS FROM  
THE FIRE II FLIGHT EXPERIMENT  
AT A REENTRY VELOCITY OF  
11.4 KILOMETERS PER SECOND

by *Dona L. Cauchon*  
*1 NASA*  
*Langley Research Center*  
*Langley Station, Hampton, Va. 3*

U. S. Government Agencies and  
Contractors Only

NATIONAL AERONAUTICS AND SPACE ADMINISTRATION

WASHINGTON, D. C. • 9 JULY 1967 10

*8 Washington, NASA 9*

3 RADIATIVE HEATING RESULTS FROM THE FIRE II FLIGHT EXPERIMENT  
AT A REENTRY VELOCITY OF 11.4 KILOMETERS PER SECOND 6

By 6 Dona L. Cauchon 8

Langley Research Center  
Langley Station, Hampton, Va.

[REDACTED]

[REDACTED]

[REDACTED]

U. S. Government Agencies and  
Contractors Only  
NATIONAL AERONAUTICS AND SPACE ADMINISTRATION

[REDACTED]

CONTENTS

	Page
SUMMARY . . . . .	1
INTRODUCTION . . . . .	1
SYMBOLS . . . . .	2
EXPERIMENT DESIGN . . . . .	6
Experimental Objectives and Design Concept . . . . .	6
Radiation Measurements . . . . .	6
EXPERIMENTAL RESULTS . . . . .	8
Total Radiometer Data . . . . .	8
Integrated Spectral Radiometer Data . . . . .	13
ANALYSIS AND DISCUSSION . . . . .	13
General . . . . .	13
First-Data-Period Experiment . . . . .	14
Second-Data-Period Experiment . . . . .	21
Third-Data-Period Experiment . . . . .	25
Additional Data Analysis . . . . .	27
Ground-Facility Experimentation . . . . .	27
Vacuum-Ultraviolet Radiation . . . . .	29
Total Heating Theory and the Fire II Results . . . . .	32
CONCLUSIONS . . . . .	33
APPENDIX A – CORRECTIONS TO RADIOMETER DATA . . . . .	34
Stagnation Radiometer . . . . .	34
Offset and Afterbody Radiometers . . . . .	36
APPENDIX B – FIRE II ERROR ANALYSIS . . . . .	38
Radiometer Calibration . . . . .	38
Flight Telemetry Error . . . . .	38
Readability of Reduced Data . . . . .	39
APPENDIX C – DATA ANALYSIS OUTSIDE PRIME DATA PERIODS . . . . .	41
REFERENCES . . . . .	44
TABLES . . . . .	48
FIGURES . . . . .	52

[REDACTED]

# RADIATIVE HEATING RESULTS FROM THE FIRE II FLIGHT EXPERIMENT AT A REENTRY VELOCITY OF 11.4 KILOMETERS PER SECOND\*

By Dona L. Cauchon  
Langley Research Center

## SUMMARY

The results of the Fire II radiation experiments on a blunt Apollo-shaped reentry package indicated values of stagnation radiative heating rate that for the flight conditions at peak heating, are predictable by existing theory. The results of ground-facility experimentation are compared with the Fire data. Changes are suggested in the existing empirical relationships for nonequilibrium radiative heating associated with early reentry.

The radiation-limiting phenomena of truncation, collision limiting, absorption, and radiation cooling, and the coupling between the radiative and convective modes of heating are analyzed from the standpoint of the Fire experiment. The stagnation radiation data present strong evidence of the dominating influence of near-infrared atomic line contributions for conditions through the time of peak heating. Significant radiation from vacuum-ultraviolet sources was indicated from a combined analysis of the calorimeter and radiometer experiments.

## INTRODUCTION

Project Fire was a flight experiment designed to measure reentry heating at hypersonic velocities. Two flights have been made along the Eastern Test Range with reentry in the vicinity of Ascension Island. Each flight provided for the launch of a powered spacecraft mounted on top of an Atlas D launch vehicle. After separation from the launch vehicle and orientation to the inertial reentry attitude, the spacecraft coasted to a point approximately 4000 nautical miles downrange. At an altitude of about 300 kilometers ( $1 \times 10^6$  feet), the reentry stage was spin-stabilized and the Antares II motor separated from the guidance components and ignited to provide a reentry speed of the order of 11.4 kilometers per second (37 000 feet per second). The 84-kilogram (185-pound) reentry package was then separated from the spent motor, which in turn was tumbled to increase its aerodynamic drag. The data-gathering portion of the flight was considered

---

[REDACTED]

[REDACTED]

[REDACTED]

to begin at an altitude of 122 kilometers (400 000 feet). The results of the first flight experiment (Fire I) have been reported in references 1 to 4.

The prime experiments of Project Fire included calorimeter measurements of total heating to the body surface and direct measurements of the gas radiance from the shock-heated air surrounding the reentry package. From the standpoint, particularly, of the radiation experiments, the second flight was considered highly desirable. The deduced Fire I stagnation radiative heating rates had favored the lower bound of theoretical prediction, but certain aspects of that experiment had caused some concern over the reliability of the results. Specifically, the interpretation of the Fire I data was immensely complicated by the presence of rather severe body motions and considerable telemetry noise and signal dropout.

The purpose of this report is to present the radiation data and deduced radiative heating rates for the Fire II experiment. Strong emphasis is placed on the stagnation heating rates and how these compare with theoretical estimates and the results of the Fire I experiment. The radiation measurements at the other radiometer locations are also discussed.

Corrections made to the radiometer data are given in appendix A. An error analysis of the Fire II data is given in appendix B. Analyses of the data obtained outside the prime data periods are discussed in appendix C.

## SYMBOLS

$B_\lambda$	Planck black-body intensity
$D$	Fire body diameter, meters
$d_{0.1}$	relaxation distance, centimeters
$d_p$	excitation distance, centimeters
$E$	flow energy, $\frac{1}{2}\rho_\infty V_\infty^3$ , watts per centimeter <sup>2</sup>
$E_t$	radiation intensity, watts per centimeter <sup>3</sup>
$F_{cl}$	collision-limiting factor (completely collision limited when $F_{cl} = 0$ ; no collision limiting when $F_{cl} = 1$ )
$F_\lambda$	spectral transmittance of inconel neutral density filters in radiometer calibration setup


$h$	altitude, kilometers (feet)
$I$	estimated gas steradiancy for flight conditions, watts per centimeter <sup>2</sup> -steradian
$I_r$	radiation steradiancy at reentry-package surface, watts per centimeter <sup>2</sup> -steradian
$I_r''$	radiation steradiancy measured at flight instrument, watts per centimeter <sup>2</sup> -steradian
$I_r'$	radiation steradiancy at flight instrument adjusted by results of postflight calibration analysis in appendix A, watts per centimeters <sup>2</sup> -steradian
$k$	shock geometry factor (assumed equal to 0.84 for Fire experiments)
$L_\lambda$	spectral transmittance of radiometer acceptance lens (or lenses)
$m$	density-scaling exponent
$N$	number of windows in equation (A2)
$n$	velocity-scaling exponent
$p$	pressure, newtons per meter <sup>2</sup> (pounds force per foot <sup>2</sup> )
$\dot{q}$	heating rate, watts per centimeter <sup>2</sup>
$\dot{q}_c$	convective heating rate, watts per centimeter <sup>2</sup>
$\dot{q}_r$	local radiative heating rate, watts per centimeter <sup>2</sup>
$R$	mean radiometer response
$R_\lambda$	spectral reflectance of radiometer beam splitter (or aluminum mirror)
$r_c$	radius at corner, meters
$r_n$	body nose radius, meters

[REDACTED]


s	distance from geometrical stagnation point measured along surface of reentry package, meters
$s_c$	distance from geometrical stagnation point to corner measured along surface of reentry package, meters
T	temperature, °K
$T_\lambda$	spectral transmittance of quartz optics in radiometer calibration setup
t	time, seconds
V	velocity, kilometers per second (feet per second)
$\alpha$	absorptivity
$\Delta t$	reentry time from 122 kilometers (400 000 feet), $t = 1617.75$ seconds; seconds
$\Delta \lambda$	wavelength interval, microns
$\delta_{ne}$	shock standoff distance (calculated to account for nonequilibrium gas effects), centimeters
$\lambda$	wavelength, microns ( $1\mu = 1 \times 10^{-6}$ meters)
$\rho$	density, kilograms per meter <sup>3</sup> (pounds mass per foot <sup>3</sup> )
$\sigma$	deviation
$\tau$	transmittance of fused quartz windows

Subscripts:

a,b	flight conditions used in scaling analysis
al	atomic line radiation
Be	beryllium (calorimeter material)



cal	calibration
cont	continuum radiation
e	pertaining to equilibrium conditions
flt	flight
mc	molecular plus continuum radiation
mean	mean value
ne	pertaining to nonequilibrium radiation
o	sea-level atmospheric conditions at Ascension Island reentry area $(T_o = 297.6^{\circ} \text{ K } (533.7^{\circ} \text{ R}); \rho_o = 1.178 \text{ kg/m}^3 (7.345 \times 10^{-2} \text{ lbm/ft}^3);$ $p_o = 1.012 \times 10^5 \text{ N/m}^2 (2113.61 \text{ lbf/ft}^2))$
off	corresponding to offset radiometer location
ref	reference conditions $(T_{\text{ref}} = 273.15^{\circ} \text{ K } (491^{\circ} \text{ R}); \rho_{\text{ref}} = 1.295 \text{ kg/m}^3$ $(8.073 \times 10^{-2} \text{ lbm/ft}^3); p_{\text{ref}} = 1.014 \times 10^5 \text{ N/m}^2 (2117.69 \text{ lbf/ft}^2))$
st	stagnation region
std	sea-level conditions for 1962 Standard Atmosphere $(T_{\text{std}} = 288.15^{\circ} \text{ K}$ $(518.67^{\circ} \text{ R}); \rho_{\text{std}} = 1.225 \text{ kg/m}^3 (7.647 \times 10^{-2} \text{ lbm/ft}^3);$ $p_{\text{std}} = 1.013 \times 10^5 \text{ N/m}^2 (2116.22 \text{ lbf/ft}^2))$
t	pertaining to total stagnation radiative heating rate including equilibrium and nonequilibrium components and corrected for truncation and collision- limiting effects
$\alpha$	total angle of attack
$\lambda$	wavelength
2	equilibrium condition behind shock
$\infty$	free-stream conditions for flight





## EXPERIMENT DESIGN

### Experimental Objectives and Design Concept

One of the primary objectives of Project Fire was to define the radiative heating environment associated with the reentry of a large-scale Apollo-shaped vehicle at a velocity of 11.4 kilometers per second (37 000 feet per second). In the concept of the Fire experiment, it was planned to measure directly the incident radiation steradiancy using onboard total radiometers. These instruments would view the gas radiation through fused quartz windows. A calorimeter experiment was also included in the scheme. The calorimeter's response to the convective plus absorbed radiative heat flux would be used in conjunction with the independent radiation measurements to deduce the convective heating component. In addition to its primary function, the calorimeter would also maintain the clean environment necessary for the radiometer experiments.

Because no single window or calorimeter material could survive the Fire reentry, the reentry package was constructed with a layered forebody consisting of three beryllium layers that served as separate calorimeters during the experiment. These layers were interspersed with three phenolic-asbestos heat shields. Quartz windows were mounted in each forebody layer to provide an optical path to the gas cap for the radiometers. The reentry package is shown in figure 1. In figure 2 are indicated the radiometer locations and the window arrays. With the use of the separate calorimeters, the reentry was broken down into three discrete experimental periods. The early reentry heating was monitored by the first beryllium layer until it reached its melting temperature. Provision was made to expose, respectively, the second and third calorimeters at about the time of peak heating and during the time of decreasing heating. The first two heat shields provided heat protection for the last two calorimeters until their designated exposure times. The third heat shield positioned behind the third calorimeter served to insulate the main body of the reentry package and to protect it in case the last calorimeter melted.

### Radiation Measurements

Total radiometers.- Direct measurements of the gas radiance from the hot plasma surrounding the reentry package were obtained with onboard radiometers. Total radiometers were placed at three locations in the reentry package. (See figs. 1 and 2.) The word "total" indicates integrated broadband measurements without spectral selectivity; the wavelength range covered by each of these instruments was from  $0.2\mu$  to  $4.0\mu$ . The radiometer sensors were gold-black flakes mounted on thermopiles. The acceptance optics included a focusing lens which imaged the source radiation upon the sensor. A reflecting  $\text{MgF}_2$ -coated aluminized mirror (or beam splitter in the case of the stagnation radiometer) served to direct the energy from the lens to the sensor in the tightly

packaged instrument. The three total radiometers used in the experiment exhibited a dynamic response of approximately 3 decades of intensity ( $0.1$  to  $100 \text{ W/cm}^2\text{-sr}$ ) without instrument saturation. The field of view of these instruments was about  $10^\circ$  (total included angle). The radiometers contained logarithmic amplifiers with direct signal output to the prescribed telemetry link for ground readout. The output of the radiometers was continuously monitored (not commutated), with provision for periodic inflight checking of the telemetry zero and full-scale signals.

One total radiometer was positioned to view the radiation to the afterbody; a second was positioned to view the radiation at a location on the spherical front face that was offset from  $16^\circ$  to  $20^\circ$  from the geometrical stagnation point (the angle varied slightly with the particular calorimeter exposed); and the third instrument was positioned to monitor the intensity of the gas at the stagnation point. The low wavelength cutoff for the total radiometer experiments was dictated by the fused-quartz windows through which the radiometers viewed the plasma radiation. The transmittance of this quartz is given in reference 1 as a function of temperature and wavelength.

Spectral radiometer.- A spectral radiometer, which shared some of the acceptance optics with the total radiometer, was also positioned at the stagnation location. This instrument was designed to monitor spectrally the  $0.2\mu$  to  $0.6\mu$  wavelength range with a resolution of  $0.004\mu$  (40 angstroms). A distinguishing feature of the spectral radiometer was a rocking diffraction grating, the motion of which alternately traversed the  $0.2\mu$  to  $0.6\mu$  spectrum of the gas cap in back and forth directions on successive scans. Optical alinement difficulties, however, limited the scans in the Fire II experiment to an analysis of the following spectral ranges: forward scan,  $0.3000\mu$  to  $0.5575\mu$ ; reverse scan,  $0.6090\mu$  to  $0.3000\mu$ . The spectra obtained from this instrument have been integrated to provide a measure of total radiation over these wavelength ranges. The individual spectra themselves are being evaluated separately and are not included in this report.

Calorimeters.- In the original concept of the Fire experiment, it had been planned to deduce the convective heating by subtracting the measured radiation (adjusted for calorimeter absorptance) from the calorimeter flux. Such a determination, however, was not possible in that not all the gas radiance incident at the calorimeter surface was "seen" by the radiometers. (Early theoretical estimates (refs. 5, 6, and 7) had indicated that the gas radiance from the stagnation region of the shock layer in front of the Fire reentry package would consist almost entirely of radiation between  $0.2\mu$  and  $2.0\mu$ . However, more recent estimates of this energy (refs. 8, 9, 10, and 11) indicated that significant levels of radiation could be expected in the spectral region below  $0.2\mu$ . For the plasma conditions associated with the Fire reentry ( $7000^\circ \text{ K} < T_2 < 11\,500^\circ \text{ K}$  and  $10^{-3} < \rho_2/\rho_{\text{ref}} < 10^{-1}$ ), the theory does not indicate any significant radiation at wavelengths longer than  $2.0\mu$ .) The results of the Fire II calorimeter measurements

[REDACTED]

published in reference 12 are further analyzed in the present paper to draw some conclusions with respect to radiation at wavelengths too short to be transmitted by the radiometer window material. The curve of spectral absorptance for the beryllium calorimeters, which was included in references 12 and 13, is shown in figure 3. Of particular significance is the strong absorbing quality of the beryllium at the lower wavelengths ( $\lambda < 0.2\mu$ ) where it becomes very sensitive to radiation.

When reduced according to the original plan, therefore, the data from the Fire II experiment assume a new connotation in that the two main ingredients for analysis are essentially: (1) the measured radiation above  $0.2\mu$  (total radiometer experiment) and (2) the combined contribution of convective heating and the absorbed radiative heating below  $0.2\mu$  (difference between the calorimeter heating rates and the radiative heating rates from the total radiometer experiment adjusted for calorimeter absorptance).

## EXPERIMENTAL RESULTS

### Total Radiometer Data

Data record.- Figure 4 shows the stagnation, offset, and afterbody radiation intensity data obtained by the three total radiometers. These data, which represent the steradiancy levels at the instruments  $I_r''$  (that is, behind the window arrays), are plotted against the elapsed time from launch. They were reduced from the original telemetry record by converting the analog voltages to steradiancy units by using the preflight calibrations for the three instruments. These records are intended solely as indicators of the general heating histories at the various body locations. Effects of small body motions and significant events such as the heat-shield ejections may also be appreciated from these reduced data. The steradiancy levels indicated in figure 4 are not, however, final values. Adjusted steradiancy values  $I_r'$  were obtained during each data period by using the methods and correction factors presented in appendix A. These corrections were deduced from the results of a postflight program which was designed to obtain more complete optical data on the various components of the radiometers and the associated calibration equipment.

As previously indicated, the forebody radiometer experiments were broken up into three discrete periods during the reentry. The outermost windows of the arrays, which were exposed to the direct heat from the hot flow field, were critical components in these experiments. The deduced heating rates were used in an iterative manner to determine the temperature distributions in these exterior windows. These distributions allowed, in turn, for proper consideration of temperature and spectral effects on window transmission. The duration of each radiometer experiment was estimated from this same procedure; the experiment was considered terminated when the calculated surface temperature of this outer window reached its melting point (approximately  $1920^\circ\text{K}$ ). The

[REDACTED]

radiometer signals did not indicate any marked increase or decrease after the computed window melting time. A condition of partial transparency persisted perhaps for some time thereafter, but it was not considered practical to attempt a calculation of these effects and expect reasonable accuracy. Based on the measured afterbody heating rates (ref. 14), the outer quartz window for that radiometer should have survived the entire reentry.

The data for the three total radiometers shown in figure 4 are continuous over the entire reentry period from 1628 to 1652 seconds. Because these data represent the steady-state radiance levels behind the window arrays measured at the instruments, they include not only the radiation levels measured during times when clean calorimeters and windows were exposed, but also data obtained during the times when the windows may have softened or melted, and when ablation products from the protective heat shields may have contaminated the flow field. Also indicated in figure 4 are the time intervals during which it was estimated that the radiometers had clearly viewed clean shocked air uncontaminated by ablation products. The lengths of these intervals represent the useful window lives prior to window surface melting which were calculated by the procedure outlined in the preceding paragraph; these time intervals essentially define the three data periods for the radiation experiments. (The times denoted in ref. 12 for the calorimeter experiments are considerably longer.) The starting times for the intervals representing the second and third experimental periods were determined from telemetered diagnostic information which indicated the approximate moment of each heat-shield ejection. These two ejections were determined to have occurred, respectively, at 1642.47 and 1648.18 seconds (elapsed times from launch). It may be noted that these two times are 0.35 second and 0.65 second later than the ejection signal times given in the Fire II trajectory report (ref. 15) for the second and third data periods, respectively. Each difference represents the finite time interval between the eject signal and the actual withdrawal of the phenolic heat shield which uncovered the clean calorimeter and radiometer window.

The telemetry records for the Fire II experiment were greatly improved over those for Fire I. There were no signal dropouts or telemetry noise to obliterate or distort the Fire II data. Modest body motions were experienced, but they were much less severe than those exhibited during the Fire I reentry where the close-proximity passage of the spent velocity package was estimated, because of shock interactions, to have contributed to the more violent high-amplitude motions. (See refs. 1, 15, and 16.) Maximum total angles of attack of about  $5^\circ$  and  $10^\circ$  were calculated to have been experienced, respectively, in the second and third data periods during the Fire II reentry. The frequencies of these motions were approximately 8 cycles/second and 12 cycles/second, respectively, in these last two data periods. The effect of the motions on the stagnation radiometer data are only mildly observable. (See fig. 4.) To adjust for these body

[REDACTED]

motion effects, the stagnation steradiancies during the second data period were smoothed by fairing across the peaks of the oscillations. This adjustment reduced the data to values essentially representative of conditions for  $0^\circ$  angle of attack. The coning type of motion (see refs. 1 and 16) experienced during both Fire reentries was such that the resulting steradiancies indicated by the offset radiometer record (on a spinning reentry package) were in the form of unsymmetrical oscillations. This condition made it difficult to determine intensity levels accurately from that record which indeed reflected the true steradiancies for that position corresponding to a  $0^\circ$  angle-of-attack entry condition. The radiation intensity at the offset radiometer location, which for the  $0^\circ$  angle-of-attack condition has fundamental value, was determined by choosing points in that trace which corresponded to times at which the stagnation record indicated peak values (or approximately  $0^\circ$  angle-of-attack conditions).

The accuracy of the data from the three forebody radiometers is estimated to be between 20 and 35 percent. The details of the error analysis are presented in appendix B.

Although the afterbody radiometer appeared to be functioning, since it responded to sporadic bursts of radiation attributed to calorimeter melting and the heat-shield ejections, the general level of radiation was apparently below its response threshold. This threshold level appeared to have shifted from the original calibration level corresponding to a heating rate of  $1\text{W}/\text{cm}^2$  to one corresponding to a minimum of  $2\text{W}/\text{cm}^2$ . This assessment was based upon the maximum  $\dot{q}_{r,\text{aft}}/\dot{q}_{r,\text{st}}$  ratio deduced from the Fire I experiment.

Calculated radiative heating rates.- The reduced steradiancies from the two forebody radiometers were converted to radiative heating rates by using the relationship:

$$\dot{q}_r = 2\pi k I_r \quad (1)$$

where  $k$ , a geometric factor to account for the curved shape of the shock front, was chosen, as in reference 1, to be 0.84 and  $I_r$  represents the adjusted radiometer steradiancy (see appendix A) corrected for window transmission, that is,

$$I_r = I_r' / \tau \quad (2)$$

where  $\tau$  is the wavelength-averaged transmission of the quartz window array and includes a consideration of the attenuating effects of temperature.

The assumptions inherent in equation (1) are those of a transparent isothermal shock layer and a concentric shock near the stagnation region. The transparent gas approximation is considered valid for the shock-layer radiation in the spectral range covered by the radiometers, that is, between  $0.2\mu$  and  $4.0\mu$ . The geometry of the shock layer associated with the Fire reentry package is such that the maximum path length

[REDACTED]

between any radiating particle in line of sight of the stagnation point and the stagnation point is less than 20 centimeters. The longer path lengths are, however, less influential because of the oblique viewing angle involved. On the basis of recently published air-radiation tables (ref. 11), path lengths up to 20 centimeters in the Fire environment would not be conducive to strong self-absorption in the gas cap at wavelengths longer than  $0.2\mu$ . Self-absorption is covered in greater detail in subsequent sections of this report. Although the steradiancy conversion factor  $2\pi k$  used in equation (1) is a good approximation for stagnation conditions, its use in reducing the offset radiometer values may reflect some inaccuracies. These inaccuracies would result primarily because of deviations from concentricity of the shock and flow-field homogeneity near the corner of the blunt Fire reentry package.

The calculated forebody radiative heating rates  $\dot{q}_{r,st}$  and  $\dot{q}_{r,off}$  deduced from the final adjusted steradiancies  $I_{r,st}$  and  $I_{r,off}$  are presented in figure 5. The steradiancies were deduced from the fairings of the original total radiometer steradiancy data as discussed in the previous section.

Fire I data scaling.- In order to compare the results of the Fire I and Fire II experiments, the Fire II stagnation heating rates that were deduced from the total radiometer data and which were shown in figure 5, are repeated in figure 6. The Fire I stagnation results are also included. It should be noted that the Fire I radiative heating rates used in this report differ from those presented in reference 1 by the instrument calibration corrections shown in appendix A. Differences in the atmosphere, flight-path angle, and velocity, and changes in the timing of the heat-shield ejections furthermore do not allow for a direct comparison of the data from the two flights on a reentry time or altitude basis. As a result, the Fire I radiative heating rates for the second and third data periods shown in figure 6 have been adjusted in order to reflect not only the instrument calibration corrections outlined in appendix A, but also to include the effects of scaling flight velocity and ambient density from the Fire I to the Fire II conditions. The scaling method of reference 13, which utilized the relationship

$$\frac{\dot{q}_{r,a}}{\dot{q}_{r,b}} = \left( \frac{V_{\infty,a}}{V_{\infty,b}} \right)^n \left( \frac{\rho_{\infty,a}}{\rho_{\infty,b}} \right)^m \quad (3)$$

with matching on reentry time from 122 kilometers, was simplified by matching the Fire I and Fire II trajectories on ambient density. This simplification reduced the density term in equation (3) to unity. The behavior of the velocity-scaling exponent  $n$  over the portion of the reentry characterized by predominantly equilibrium radiation was determined by using the theoretical values of radiative heating ( $\lambda > 0.2\mu$ ) from reference 11. That is, at the Fire I reentry conditions  $V_{\infty,a}$  and  $\rho_{\infty,a}$ , the theoretical

[REDACTED]

[REDACTED]

stagnation equilibrium radiative heating rate  $\dot{q}_{r,a}$  was determined from reference 11. Similarly, at the Fire II reentry conditions to which it was desired to scale the Fire I results,  $V_{\infty,b}$  and  $\rho_{\infty,b}$  (but where  $\rho_{\infty,b} = \rho_{\infty,a}$  as the matching parameter), theoretical values of  $\dot{q}_{r,b}$  were determined. From these results, values of  $n$  were determined for the entire range of reentry conditions by using equation (3). The resulting variation of  $n$  with ambient density is indicated in figure 7.

The Fire I radiative heating rates ( $\lambda > 0.2\mu$ ) for the second and third data periods were scaled to Fire II velocities in figure 6 by using the relationship indicated in figure 7. This relationship for the velocity-scaling exponent  $n$  was doublechecked for verification by a calculation similar to that outlined above in which the Fire II data were scaled to the Fire I conditions. It is also interesting to note that an identical scaling analysis using the theory of reference 8 for  $\lambda > 0.2\mu$ , which does not consider the near-infrared atomic line radiation, produced the same velocity-scaling relationship.

Additional scaling calculations in which the Fire I and Fire II velocities were matched indicated a constant value of  $m$  equal to 1.7 to be a reasonable approximation of the density-scaling exponent over the range of velocities from 7.5 to 11.3 kilometers per second (approximately 25 000 to 37 000 feet per second). It should be noted that in using the Fire trajectories to determine the velocity-scaling relationship in figure 7, the data were defined by a unique combination of velocity and ambient density conditions and should not be considered to be a generalized curve.

The validity of the results of the scaling procedure was dependent upon the accuracy to which the Fire trajectories and atmospheric data were determined. The Space Physics Research Laboratory, University of Michigan, which reduced the sounding data, estimated the accuracy of the Ascension atmosphere to be  $\pm 5$  percent for pressure and density, and  $\pm 5^\circ$  K for temperature. The trajectories were determined from an inhouse computer program (refs. 4 and 15) which simulated the blacked-out portion of the reentry between the radar-measured segments obtained before loss of the tracking beacon signal and after it was reacquired. Altitude and velocity, as determined from the tracking radar, were estimated by the Eastern Test Range to be accurate within  $\pm 30$  m and  $\pm 8$  m/sec, respectively, for the portions of the trajectory bracketing the Fire heating experiment.

Scaling the first data period results by the aforementioned techniques is probably not too reliable because of the nonequilibrium condition of the reentry package shock layer during most of that period. These Fire I data, as a result, have not been scaled in figure 6. The data have been matched instead on ambient density and a converse approach used – that of determining the velocity-scaling exponent  $n$  from the two sets of flight data. The density was particularly appropriate as the matching parameter at

[REDACTED]

these flight conditions because of the apparently strong density-dependent truncation and collision-limiting effects estimated for the early portion of the reentry.

### Integrated Spectral Radiometer Data

Heating rates determined from integrations of the scans of the spectral radiometer steradiancy data and adjusted for window transmission and shock shape effects have been included in figure 5. The heating rates obtained from the forward and reverse scans are indicated separately. Instrument sensitivity at the low steradiancy levels led to considerable scatter in the data during the first experimental period.

## ANALYSIS AND DISCUSSION

### General

In reference 1, the Fire I results were compared with estimates based on several prominent equilibrium radiation theories (refs. 5, 6, 7, and 8) and empirical nonequilibrium relationships (refs. 17 and 18). The continual assessment of hot-air radiation, however, has resulted in new and revised theories (refs. 9, 10, and 11) in which the level and structure of the equilibrium radiation have considerably changed. Vacuum-ultraviolet radiation ( $\lambda < 0.2\mu$ ), consisting of both continuum and atomic line contributions, is now estimated to provide a strong influence on reentry heating. For the Fire environment, radiation from near-infrared atomic lines is estimated (ref. 11) to be greater than that from other radiating sources at  $\lambda > 0.2\mu$  at the peak heating conditions. The radiation-limiting effects of self-absorption and radiation cooling have received considerable attention and theories on the associated coupling effects between the radiative and convective modes of heating are being advanced. The Fire I results showed that nonequilibrium radiation appeared to be reasonably predictable up to Fire velocities by the method of reference 18. Also, the effects of the radiation-limiting phenomena of truncation and collision limiting for early reentry conditions at these velocities appeared to be predictable by the methods discussed in references 1, 17, and 18.

In this section of the report, the Fire II results are evaluated from the standpoint of the aforementioned theory. Comparisons between the Fire II and the Fire I results and ground-facility experimentation are also made. Because of the changing nature of the radiation and the different radiation-limiting phenomena that operate at particular times during the varying conditions of reentry, each data period is analyzed separately as a unique experiment. The emphasis is on the stagnation experiments. However, the off-set radiometer results and forebody distributions are also covered. The radiation level incident at the afterbody total radiometer was generally too low to be recorded, and is not discussed further.



### First-Data-Period Experiment

Experiment conditions.- The first-data-period experiment consisted of obtaining measurements of radiation steradiancy at two locations on the forebody of the Fire reentry package. These steradiancies obtained at the previously defined stagnation and offset positions were then converted to heating rates by using the methods outlined in the section "Experimental Results." The starting and ending conditions for the continuous stagnation experiment were:

Condition	Elapsed time, sec	Altitude, km (feet)	Velocity, km/sec (fps)	$\rho_{\infty}/\rho_0$	$\rho_{\infty}/\rho_{std}$
Starting	1631.30	83.75 (274 800)	11.37 (37 312)	$8.88 \times 10^{-6}$	$8.52 \times 10^{-6}$
Ending	1636.47	69.80 (229 000)	11.30 (37 060)	$8.60 \times 10^{-5}$	$8.25 \times 10^{-5}$

(The starting conditions for the radiation experiments of this data period were essentially governed by the threshold sensitivity of the radiometers.) Prior to  $t = 1634$  seconds, the stagnation flow field and the radiation therefrom were estimated to be in a wholly nonequilibrium state. At  $t = 1634.2$  seconds, it was indicated from calculations based on the method and data of reference 17 that  $d_{0,1} \approx 0.75\delta_{ne}$ , the criterion chosen by Page and Arnold (ref. 18) at which to define incipient truncation at the stagnation region. After this time, the shorter excitation and relaxation times in the shock-layer flow and attendant decrease in nonequilibrium zone thickness gave rise to increasing contributions from equilibrium sources. By 1636 seconds, the equilibrium radiation was indicated by the theory to be contributing about 70 percent of the total stagnation radiative heating at wavelengths longer than  $0.2\mu$ . On the basis of theoretical estimates, therefore, the first-data-period stagnation experiment spanned from a condition of wholly nonequilibrium flow to one of strong equilibrium influence.

The results of this first data period for Fire II are indicated in figures 5 and 6. The density-matched first data period results for Fire I are also included in figure 6. At  $t \lesssim 1634$  seconds, the radiation-limiting effects of truncation and collision limiting were estimated to provide significant attenuation of the base radiative heating rates (that is, rates predictable from the empirical nonequilibrium estimates of ref. 18). These predicted effects based on the Fire II trajectory are indicated in table I. The probable effect of radiation cooling on the stagnation radiative heating rate during the latter part of the first data-period experiment is discussed in a subsequent section of the report. The radiation-limiting analyses for the first data period are restricted primarily to the wavelength range,  $\lambda > 0.2\mu$ .

Truncation and collision limiting.- The single "solid" theory line denoted in figure 6 for the early reentry (up to  $t = 1634$  seconds) includes the estimated truncation

[REDACTED]

effect on the nonequilibrium levels based on reference 18. The untruncated nonequilibrium radiative heating rate for this constant-velocity time period was indicated by the density-independent relationship of reference 18 to be 15.2 watts per centimeter<sup>2</sup>. Although other radiation-limiting (or radiation-enhancing) phenomena, such as nonequilibrium radiation cooling, absorption of energy in the free stream, etc., may be contributing at these early flight conditions, the theory in these areas has not been sufficiently developed at this time to allow for any realistic appraisal of their effects. In the absence, therefore, of any such quantitative information, the ratios of the measured Fire II radiative heating rates to the radiation theory for  $\lambda > 0.2\mu$  (adjusted as indicated for truncation) during the first data period were taken to be a measure of the collision-limiting effect. Similar ratios were calculated between the Fire I results and the theory for the Fire I entry conditions (see ref. 1). These ratios have been expressed in the form of collision-limiting factors  $F_{cl}$  in this report.

The Fire I heating rates in figure 6 are indicated to be between 2 and 3 times higher than the levels of the Fire II experiment. By the nature of the calculations, the collision-limiting factors for the two flights were affected in a similar manner. These factors are shown plotted against ambient density ratio  $\rho_{\infty}/\rho_0$  in figure 8. It should be emphasized that this collision-limiting effect indicated by the Fire data was established solely on the basis of measurements obtained at wavelengths longer than  $0.2\mu$ . In addition to the calculated values of  $F_{cl}$  for the two Fire flight experiments, two points resulting from shock-tube experiments (ref. 17) on one molecular-band system ( $N_2^+$  first negative) at a velocity of 5.5 km/sec are also included in figure 8. Up to the time of the Fire experiments, these low-speed data were essentially all that were available on collision limiting. The flight data from the Fire experiments were actually continuous; the discrete points indicated by the symbols in figure 8 are samplings of those data. (It may be noted that the Fire I collision-limiting trace differs slightly from that indicated in reference 1. This variation resulted in part from the change in measured radiation levels occasioned by the application of the radiometer calibration corrections presented in appendix A. As a result, the Fire I trace in figure 8 supervenes that of the reference 1 report. The trace was additionally influenced by the fact that the actual Fire I stagnation radiometer data were used in the calculations of these collision-limiting factors. In reference 1, because of the uncertainty concerning the relative levels indicated by the two forebody radiometers, an average fairing between the data from these two instruments had been used. In the Fire I calculations in this report, values of  $F_{cl}$  were not allowed to exceed a value of 1.0.)

Radiation cooling.- The falloff in the calculated Fire II collision-limiting values in figure 8 after  $t = 1634$  seconds ( $\rho_{\infty}/\rho_0 = 3.16 \times 10^{-5}$ ) resulted from the increasing values of the theoretical equilibrium radiation component of reference 11. That theory, which accounts for radiation from an isothermal, absorbing gas layer, does not include a

[REDACTED]

consideration of radiation cooling. Hoshizaki and Wilson (ref. 19) have estimated this radiation-cooling effect to be slight (about 10 percent) for the conditions corresponding to these later times in the Fire II first experimental period ( $h = 70$  km (230 000 feet),  $V_\infty = 11.3$  km/sec (37 000 feet per second)). It should be emphasized however that the results of Hoshizaki and Wilson are not wholly compatible with the theory of Allen (ref. 11) for two reasons: (1) reference 19 does not include atomic line radiation in its analysis, and (2) the body size is larger for the reference 19 study. Furthermore, the radiation cooling deduced from reference 19 applies to the entire wave length range. The results inferred from the Fire experiments are for  $\lambda > 0.2\mu$  and any comparisons must be tempered accordingly.

Support for the conclusion that radiation cooling might be limiting, however, at these flight conditions is afforded by the calculated value of the radiation-cooling parameter  $\gamma$ . This parameter, defined by the ratio of the radiation loss from the gas cap to the total available flow energy ( $\gamma = 2\dot{q}_r/E$ ), has been used commonly as the criterion for estimating the effect of radiation cooling on the theoretical heating rate which does not include a consideration of this effect. (Values of  $\gamma > 0.01$  are, in general, indicative of consideration.) Although radiation cooling is indicated on this basis to be actively limiting during the latter part of the first data period ( $t > 1634$  seconds), it is difficult to assign any quantitative value to its effect at these flight conditions. As a result, no attempt will be made here to separate the radiation-limiting effects of collision limiting and radiation cooling. Cooling must be recognized as a possible contributing influence but, for the purposes of this report, its effect will be included in the radiation-limiting estimate indicated by the collision-limiting factor  $F_{cl}$  in figure 8.

Theory and Fire results.- One aspect of the first experimental period data was the wide variation between the Fire I and Fire II results. In the Fire I analysis (ref. 1), telemetry and body motion problems made the data reduction for the second and third data periods more difficult. However, the first data period was not affected by body motion problems and therefore held to be reliable where not affected by the telemetry noise and signal dropout. Because of the unrealistic distribution of radiation over the reentry-package forebody indicated by the Fire I radiometer data, there had been a tendency to question the reliability of the Fire I instruments. In that experiment, the offset radiometer had indicated levels of radiation that were higher than the recorded stagnation levels. As a result, it could not be concluded positively which of the two radiometers (or possibly both) was in error. The Fire II data not only indicated a more realistic forebody distribution of radiation but, more importantly, provided a measure by which the accuracy of the Fire I instruments could be evaluated. In figures 5 and 9 are plotted the integrated spectral radiometer scans for the first experimental period of Fire II. Scans from the first experimental period of Fire I and the corresponding spectral ranges are also shown in figure 9. As in the case of the total radiometer results, the Fire I

[REDACTED]

spectral data have been compared with the Fire II data at the same ambient density. The units of  $W/cm^2\text{-sr}$  used in figure 9 are representative of the gas steradiancy outside the window array at the surface of the reentry package. The time scale is the elapsed time from launch for the Fire II trajectory. The smaller number of Fire I points resulted from the dropouts in the sporadic telemetry signal. An estimate of the effect of telemetry and instrument system noise at low signal levels was deduced from the spectral radiometer records. The fairings indicated in figure 9 for the two sets of data were determined from the use of selected spectra which were essentially free of noise. Figure 9 shows that the Fire I steradiancies (and heating rates) obtained from the spectral radiometer over essentially comparable wavelength ranges are a factor of about 3 higher than those for Fire II. This ratio agrees well with the stagnation total radiometer results for the two flights. This agreement exhibited by both stagnation radiometers for the two flights points up a very convincing argument for the integrity of the Fire I stagnation total radiometer and essentially authenticates the data resulting therefrom. One is led, as a result of comparing the Fire I and Fire II data, to conclude that the Fire I heating rates, matched at the Fire II ambient-density conditions, are indeed a factor of 2 to 3 times higher than those for Fire II. The results from the two flight experiments, therefore, imply a much higher velocity dependence of nonequilibrium radiative heating than is indicated from the empirical method of reference 18. It would appear that no significant change occurred in the broad spectral breakdown of radiation at  $\lambda > 0.2\mu$  as the absolute levels increased with time during the first-data-period experiments. This result is supported by the fact that the percentage of radiation above  $0.2\mu$  that lies between  $0.2\mu$  and  $0.6\mu$  in each flight experiment remained about the same throughout the entire first data period.

An analysis was generated in order to effect a more meaningful comparison between the estimates of nonequilibrium radiative heating based on reference 18 and the Fire results. In figure 10, a solid line is used to indicate the fairing of reference 18 of the experimental ground-facility work of references 17, 18, 20, 21, and 22. This straight line indicates a fourth-power velocity dependence of nonequilibrium radiative heating. The calculations involved in the Project Fire collision-limiting analysis, however, served to support the notion of a stronger velocity dependence. It is recalled that the values of  $F_{cl}$  in figure 8 (for  $t < 1634$  seconds) were defined by the ratio of the Fire radiative heating rates ( $\lambda > 0.2\mu$ ) to the reference 18 theory. If the fairing of the ground-facility data in figure 10 had been such as to indicate a steeper velocity dependence of nonequilibrium radiation at the Fire velocities, a better agreement between the collision-limiting factors for the Fire I and Fire II experiments could have been obtained in figure 8. Calculations were performed in which the slope for the nonequilibrium radiation-velocity relationship between 11 km/sec and 12 km/sec was varied iteratively while observing the behavior of the collision-limiting factors in figure 8. These calculations

resulted in the selection of a new fairing for the ground-facility data summarized in reference 18. This new fairing is indicated by the dashed curve in figure 10 and reflects approximately a ninth-power velocity dependence of nonequilibrium radiative heating at the Fire velocities. The changes in the collision-limiting factors as a result of the revised fairing are shown in figure 10. From a consideration of the new experimental data from the Fire experiments and the two reference 17 points, what was estimated to be a representative collision-limiting relationship was chosen; this fairing is indicated as the dashed curve in figure 11. The weighting of the Fire II data in the collision-limiting analysis tends to alter slightly the relationship suggested in reference 1. The revised version – that corresponding to the collision-limiting fairing in figure 11 – may be defined by the following set of equations:

$$\left. \begin{aligned} F_{cl} &= 0, \left( \rho_{\infty}/\rho_0 \right) \leq 6.92 \times 10^{-6} \\ F_{cl} &= 1.486 \left( \log \rho_{\infty}/\rho_0 + 5.16 \right)^2, 6.92 \times 10^{-6} \leq \left( \rho_{\infty}/\rho_0 \right) \leq 2.63 \times 10^{-5} \\ F_{cl} &= 1 - 1.486 \left( \log \rho_{\infty}/\rho_0 + 4.00 \right)^2, 2.63 \times 10^{-5} \leq \left( \rho_{\infty}/\rho_0 \right) \leq 10^{-4} \\ F_{cl} &= 1.0, \left( \rho_{\infty}/\rho_0 \right) \geq 10^{-4} \end{aligned} \right\} \quad (4)$$

The Fire I and Fire II results have been added to figure 10. The data correspond to the condition of incipient truncation  $d_{0.1} = 0.75\delta_{ne}$  which was estimated to have occurred at a Fire II time of 1634.2 seconds. (Matching the Fire I and Fire II data at the condition of incipient truncation closely approximates a matching on ambient or free-stream density.) The Fire data and the pertinent flight parameters are shown in the following table:

Fire II time, sec	Radiative heating rates, W/cm <sup>2</sup>		V <sub>∞</sub> , km/sec		$\rho_{\infty}/\rho_0$
	Fire I	Fire II	Fire I	Fire II	
1634.2	20.0	8.40	11.57	11.36	$3.50 \times 10^{-5}$

On the basis of the ambient conditions specified in reference 17, the ground-facility data indicated in figure 10 were essentially unaffected by collision limiting. These data were reduced on the basis of a parallel-plane gas-layer geometry. In order to make the Fire results compatible with the ground-facility data in figure 10, it was necessary to negate the effects of collision limiting and geometry inherent in the Fire results. The data (and relationships) of figure 10 may thereby be considered base values of nonequilibrium

radiative heating to which any necessary radiation-limiting corrections for all flight conditions may be subsequently applied. To make the adjustments, the Fire radiative heating rates in the above table were divided by the products of the geometry and collision-limiting values used in the Fire analysis. These values are indicated in the following table:

ADJUSTMENT VALUES

①	②	③	④	⑤	⑥	⑦
Experiment	Fire radiative heating rate, W/cm <sup>2</sup>	Geometry	Collision-limiting $\dot{q}_e + \dot{q}_{ne}$	Collision-limiting $\dot{q}_{ne}$ only	Product ③ × ⑤	Adjusted Fire heating rates, W/cm <sup>2</sup> ② ÷ ⑥
Fire I	20.0	0.84	{ 0.70 .87	0.70 .99	0.59 .83	33.9 24.1
Fire II	8.4	.84	{ .70 .47	.70 .56	.59 .47	14.2 17.9

The two collision-limiting factors given in column ④ for each data entry in the table were obtained from figure 11 from the estimated relationship (defined by eq. (4)) and the actual "data" curve, respectively. Since the actual "data" curves in figure 11 include a consideration of both the nonequilibrium and equilibrium theory, a revised collision-limiting factor has been calculated in column ⑤ for use only with the nonequilibrium theory at  $t = 1634.2$  seconds. The spread resulting from the use of the maximum and minimum factors for each experiment was estimated to reflect the limits of accuracy in the adjusted Fire data.

The method of using the actual data curves in figure 11 to determine one such limit is inherently redundant because of the nature of the calculation of the collision-limiting factors in that figure. However, if it is assumed that collision limiting is a unique function of free-stream density (as suggested by ref. 17) and can be defined by the long-dashed fairing in figure 11 (or eq. (4)), then the Fire I and Fire II results in figure 11 may be considered experimental scatter about this unique relationship. On this basis, the collision-limiting factors from the Fire I "data" curve in figure 11 may be considered maximum values and those from the Fire II "data" curve minimum values. Therefore, from the calculations described, one limit in the spread of the adjusted Fire data in figure 10 would fall on the ninth-power velocity-dependent theory curve.

The adjusted Fire results are shown in figure 10. It is important to note that an extrapolation of the revised relationship in figure 10 to interplanetary return velocities of 15 to 18 km/sec (50 000 to 60 000 fps) would result in a very significant increase in

[REDACTED]

the estimated nonequilibrium radiative heating contribution over that resulting from a similar extrapolation of the method of reference 18.

Spectral radiometer data analysis.- The integrated spectral radiometer data for the first experimental period exhibited considerable scatter during the early portion of that period. (See fig. 5.) This scatter was attributed to instrument sensitivity at essentially threshold values of radiation. Later in the experiment ( $t \approx 1636$  sec), the scatter essentially disappeared and the integrated spectral scans ( $0.3\mu < \lambda < 0.609\mu$  for reverse scans) exhibited levels of radiation that were about 16 percent of those indicated by the total radiometer. About 8 percent of the radiation above  $0.2\mu$  is estimated from the theory to occur between  $0.2\mu$  and  $0.3\mu$ . Radiation from sources at wavelengths longer than  $0.609\mu$  therefore is indicated to contribute about three-quarters of the radiant energy above  $0.2\mu$  at the stagnation point at this particular time in the reentry. If an allowance is made for the continuum radiation above  $0.609\mu$  and also for the questionable state of the nonequilibrium gas, this proportion is in fair agreement with the equilibrium levels estimated from reference 11 (see table I) which predict for these conditions strong dominating atomic line contributions (65 percent) in the near infrared. Despite the scatter in the spectral radiometer integrations at times prior to  $t = 1635$  seconds, the presence of strong near-infrared contributions at nonequilibrium flow conditions is nevertheless implied also during the earlier times associated with nonequilibrium flow.

Forebody radiative heating distribution.- The offset radiometer in the Fire II experiment indicated a level of radiation that was about 80 percent of the stagnation value at  $t = 1633$  seconds in the first data period. (See fig. 5.) Nonequilibrium radiative heating distributions across the front face of the Fire reentry package have been estimated for approximately the same reentry conditions by references 23 and 24. These theoretical flow-field studies indicate values of incident radiation at the offset radiometer location that are 94 and 97 percent of the stagnation value, respectively. (See fig. 9 in ref. 1.) It should be pointed out that the distribution of radiant energy in the shock layer across the front face of the Fire reentry package is dependent upon the thermodynamic state and species concentration in the flow. Total radiation estimates (or measurements) further imply specific spectral distributions. The theoretical studies of references 23 and 24, by the nature of some of the assumptions used (equilibrium concentrations) and species neglected (atomic lines), cannot be considered as directly comparable with the Fire results. These theoretical works are referenced in order to inform the reader of the availability of detailed flow-field studies that were carried out prior to Fire II for almost the precise conditions of the flight experiment.

## Second-Data-Period Experiment

Experiment conditions.- The forebody experiments of the second data period of Project Fire were characterized principally by equilibrium radiation. The starting and ending conditions for the continuous stagnation experiment were:

Conditions	Elapsed time	Altitude, km (feet)	Velocity, km/sec (fps)	$\rho_{\infty}/\rho_0$	$\rho_{\infty}/\rho_{std}$
Starting	1642.47	54.34 (178 200)	10.61 (34 815)	$5.75 \times 10^{-4}$	$5.42 \times 10^{-4}$
Ending	1642.90	53.23 (174 700)	10.50 (34 460)	$6.45 \times 10^{-4}$	$6.18 \times 10^{-4}$

Spectral radiometer data analysis.- The integrated spectral radiometer record (fig. 5) tends to keynote the analysis of the Fire data in this second data period. These integrations of the spectral measurements at the stagnation point indicate that of the radiation above  $0.2\mu$  monitored by the total radiometer, only about 17 percent lies in the  $0.30\mu$  to  $0.609\mu$  wavelength range of the spectral instrument. On the basis of a theoretical spectral distribution of molecular and continuum radiation (ref. 7), which was augmented by near-infrared atomic line estimates from reference 11, about 9 percent of the incident radiation during the second data period experiment is estimated to have occurred in the  $0.2\mu$  to  $0.3\mu$  range. From this analysis, therefore, it was determined that in the stagnation region some three-quarters of the radiant energy above  $0.2\mu$  occurred at wavelengths longer than  $0.609\mu$ . The Allen theory, which for these conditions indicates that about 63 percent of the energy at  $\lambda > 0.2\mu$  results from atomic line radiation (practically all of which occurs at  $\lambda > 0.609\mu$ ), is in good agreement in a broadband spectral sense with the Fire results. The continuum radiation occurring at  $\lambda > 0.609\mu$  would furthermore make the 63-percent value a lower limit for total radiation in that wavelength region.

The second-data-period and latter portions of the first-data-period experiments were characterized by equilibrium gas cap temperatures greater than  $10\,000^{\circ}\text{K}$ . The estimates of reference 11 of strong contributions from the near-infrared lines at these temperatures appear therefore to be well supported by these Fire experiments.

Total radiometer data analysis.- The Fire II stagnation radiative heating rates deduced from the total radiometer at that position are shown in figure 6. The levels range from about  $325\text{ W/cm}^2$  to  $335\text{ W/cm}^2$  over this experimental period. In making theoretical comparisons with these Fire results, it is important to note the differences in the spectral ranges covered by the theories and the Fire experiment. The Fire experiment covered all radiation between  $0.2\mu$  and  $4.0\mu$ . This experiment is easily compared with Allen's theory (ref. 11) which presents a breakdown of radiation above and below  $0.2\mu$ . Reference 11 further distinguishes between the continuum and atomic



line contributions in each region and presents estimates on molecular radiation. Biberman et al. (ref. 10), on the other hand, present their theory with a separation of continuum radiation at  $0.125\mu$ . Although line radiation is considered, the breakdown in reference 10 is between "integrated weak lines" and "individual strong lines." The contributions from each of these groups of lines are included in the ultraviolet, visible, and infrared portions of the spectrum and thus make the estimates more difficult to compare with the Fire experiments. Ionic line radiation in the vacuum-ultraviolet region is also included in the reference 10 analysis. The radiation at  $\lambda > 0.2\mu$  for the Biberman theory has been approximated by assuming that the ratio between the Biberman and Allen theories for  $\lambda > 0.2\mu$  is the same as that for the two theories over the entire spectrum. These estimated values for the Biberman theory are tabulated in column (29) of table I. Although Biberman and Allen used different f-numbers and cross sections in their computations, the broad percentage breakdown of radiation (based on a 10-cm layer thickness) appears to indicate reasonable agreement (within 20 percent) between the various contributors at the Fire conditions. (See the following table.)

#### PERCENT CONTRIBUTION OF VARIOUS RADIATING SOURCES

[Conditions:  $T_2 = 11\ 000^\circ\text{K}$ ,  $\rho_2/\rho_{\text{ref}} = 10^{-2}$ ,  $p_2 \approx 1\text{ atm}$ ]

Allen (ref. 11)	Percent contribution	Biberman, et al. (ref. 10)	Percent contribution
Continuum, $\lambda < 0.2\mu$	10	Continuum, $\lambda < 0.125\mu$	12
Lines, $\lambda < 0.2\mu$	30	All lines (atomic and ionic) }	50
Lines, $\lambda > 0.2\mu$	32		
Continuum, $\lambda > 0.2\mu$	28	Continuum, $\lambda > 0.125\mu$	38

The values of radiation over the entire spectrum for references 10 and 11 are tabulated in columns (25) and (24), respectively, of table I. Because of the apparent transparency of the plasma at  $\lambda > 0.2\mu$  at the Fire conditions, a geometric factor of 0.84 has also been considered in the determination of the radiative heating rates in that wavelength region which are tabulated in columns (28) and (29) of table I.


It is possible to consider other theoretical works (refs. 6, 7, and 8) that from the standpoint of the total intensity level at  $\lambda > 0.2\mu$ , may be in equally good agreement with the Fire results. The theoretical levels from references 6, 7, and 8 for the Fire trajectory are presented in table I in columns (18), (17), and (19), respectively. None of these references, however, considers atomic line radiation. It would appear that the levels predictable from reference 8 are in particularly good accord with the Fire results. It

must be pointed out in the analysis, however, that there are dangers in making unrestricted comparisons and that care should be exercised in drawing conclusions therefrom. The theoretical comparisons suggested in table I are not without such restrictions.

The Allen and Biberman theories, although probably the most complete available (in that each considers practically all the acknowledged radiating sources), are based on an isothermal gas slab and do not include a consideration of shock curvature and the potentially strong effects of radiation cooling. References 6, 7, and 8 are based on similar approximations. In order to provide some dependable basis for comparison between the theory and the Fire results, an evaluation has been made of the effects of radiation cooling (with absorption) on the stagnation heating rates for this second-data-period experiment.

Theoretical treatments of radiation cooling in an absorbing gas and the attendant coupling between the radiative and convective modes of heating have been published in references 19 and 25. These efforts reflect a more realistic approach to the problem; previously, Goulard (ref. 26) had estimated the effects of these phenomena in a transparent medium. The discussion of radiation cooling and coupling in this report, however, will rely heavily on the work of Olstad (ref. 27). Olstad's method was based on a nongray, absorbing gas model and was directed to a study of the exact Fire conditions. It is not correct to consider adjustments to such as the references 10 and reference 11 theories directly by factors obtained from either references 19 or 25 for two reasons: first, the basic radiation theories assumed in those references were not those of either reference 10 or 11 and did not include a consideration of atomic line radiation. The profiles of thermodynamic properties in the flow at the stagnation point depend upon the basic radiation sources assumed when radiation loss is to be considered. Reference 25 was restricted furthermore to a gray gas model. The second reason for not applying the theories of references 19 and 25 to the previously mentioned theoretical levels is the incompatibility of such a radiation-cooling adjustment in the abbreviated wavelength range associated with the Fire radiation experiment. As previously mentioned, all radiating sources must be considered in making an estimate of radiation loss with absorption. The effects deduced in references 19 and 25 are for the entire spectrum which includes the vacuum ultraviolet. To apply any such correction to a particular wavelength increment (in this instance, Fire,  $0.2\mu < \lambda < 4.0\mu$ ) is incorrect. The radiation above  $0.2\mu$  is essentially unaffected by self-absorption and, although weighted in the calculations for the complete spectrum, may not necessarily reflect the radiation-cooling effect so deduced.

Except for replacing the vacuum-ultraviolet estimate of free-bound radiation of reference 11 with that of reference 9, the work of reference 27 has been based on the source radiation estimated from reference 11 over the entire spectrum. Using his small



perturbation method, Olstad (ref. 27) made calculations for the conditions corresponding to the second data period of the Fire experiment. The results of these calculations indicated that at wavelengths longer than  $0.2\mu$ , the stagnation radiative heating rate based on the isothermal absorbing gas model of Allen (ref. 11) should be multiplied by a factor of 0.70 to account for radiation cooling. This reduction is approximately 6 percent less severe than that estimated from the factor calculated for the entire spectrum (0.66). The radiation-cooling effect calculated for the  $\lambda > 0.2\mu$  spectral region lowers the theoretical levels of Allen at those wavelengths to values in close agreement with the Fire II results. The theoretical estimates of Allen (ref. 11) of the stagnation, radiative heating rates at  $\lambda > 0.2\mu$  are compared in figure 6 with the Fire results for the complete reentry. These equilibrium radiation estimates have been supplemented by an allowance for nonequilibrium radiation obtained from reference 18 and adjusted, where applicable, for collision limiting according to equation (4). This theory, which is indicated by the continuous line in figure 6 does not include any consideration of the radiation-cooling effect. The results of the cooling analysis performed by Olstad for the conditions at the beginning of the second data period are indicated by a symbol in figure 6 which shows a stagnation radiative heating rate for  $\lambda > 0.2\mu$  of 340 watts per centimeter<sup>2</sup>. The radiation cooling calculated by Olstad for the entire spectrum and which included line radiation was more severe than that indicated by the correlation of Gruszczynski and Warren (ref. 28) of the results of references 19 and 25 which did not consider the lines. The theoretical broadband breakdown of radiation at wavelengths longer than  $0.2\mu$  (that is, above and below  $0.6\mu$ ) that was discussed in the preceding spectral radiometer data analysis section was based on the assumption of an isothermal absorbing gas. Although the Olstad analysis suggests a rather strong temperature gradient in the stagnation flow field near the wall, the spectral distribution of radiation at the wall was not expected to be affected greatly by the radiation-cooling effect. It is reasonable to assume that the transparency of the plasma at  $\lambda > 0.2\mu$  would permit the higher temperature plasma away from the immediate wall area to influence a higher average temperature field than would be the case in a strongly absorbing gas.

It is concluded therefore from the Fire II experiment that, for reentry conditions corresponding to the second data period, the estimates of stagnation equilibrium radiative heating rates based on Allen (ref. 11) are high by a factor of 1.5. Since the theory does not consider the limiting effect of radiation cooling, it is at least overestimated to that degree. The radiation-cooling effect deduced by Olstad (ref. 27) would tend to bring the reference 11 levels shown in figure 6 into very close agreement with the Fire results.

Comparisons of the Fire results for the second and third data periods with the data obtained from ground facilities are deferred until after the discussion of the third-data-period experiment.

Forebody radiative heating distribution.- The offset radiometer in the Fire II experiment indicated levels of radiation that were approximately 60 percent of the stagnation values during the second data period. (See fig. 5.) The equilibrium radiative heating rate at the offset radiometer location on the reentry package was indicated from the Project Fire flow-field studies (refs. 23, 24, 29, and 30) to be, respectively, 0.64, 0.34, 0.60, and 0.40 of the stagnation value at flight conditions similar to those of the second data period. The estimates of references 23 and 29 appear to be in better accord with the Fire results for the offset radiometer. However, as in the case of the first data period, atomic line radiation was neglected in the theoretical studies, and such differences in the theoretical and experimental energy distributions must serve to temper any such comparisons.

### Third-Data-Period Experiment

Experiment conditions.- The third experimental period consisted of continuous measurements of the reentry environment that like the second data period was characterized by radiation at equilibrium conditions. The starting and ending flight conditions for this experiment period were:

Conditions	Elapsed time, sec	Altitude, km (feet)	Velocity, km/sec (fps)	$\rho_{\infty}/\rho_0$	$\rho_{\infty}/\rho_{std}$
Starting	1648.16	41.80 (137 100)	8.20 (26 910)	$2.65 \times 10^{-3}$	$2.54 \times 10^{-3}$
Ending	1648.50	41.19 (135 100)	7.96 (26 185)	$2.90 \times 10^{-3}$	$2.78 \times 10^{-3}$

(The calculation for the condition of surface melting of the outer quartz window indicated that this experiment should have lasted to 1648.84 seconds. However, the records indicated erratic behavior characteristic of window melting at 1648.50 seconds. It was felt that inasmuch as the first 0.34 second of data was adequate from the standpoint of the experiment, nothing was to be gained by using the uncertain data after 1648.50 seconds.)

Spectral radiometer data analysis.- The third-data-period experiment, although conducted at conditions associated with equilibrium radiation, differed from the second-data-period experiment in that radiation from molecular band systems was expected to dominate. This molecular radiation coupled with a corresponding decrease in line radiation was expected to produce a spectral distribution of energy which would differ considerably from that of the first and second experimental periods. The integrated spectral radiometer scans indicated that of the radiation occurring above  $0.2\mu$ , approximately 55 percent fell in the  $0.3\mu$  to  $0.609\mu$  wavelength range at the beginning conditions of the experiment. The radiation contribution from the same spectral region had increased to about 70 percent at the ending conditions.

For conditions corresponding to the start of the third data period experiment, theoretical broadband spectral distributions of air radiation for  $\lambda > 0.2\mu$  (based on the Allen and Breene and Nardone theories) are indicated in the following table. The corresponding Fire II results are also given.

$\Delta\lambda$	Radiation intensity (refs. 11 and 31)	(Refs. 5 and 8)	Fire II data
$0.2\mu < \lambda < 0.3\mu$	15 percent	20 percent	15 percent
$0.3\mu < \lambda < 0.6\mu$	35 percent	45 percent	55 percent
$0.6\mu < \lambda < 4.0\mu$	50 percent	35 percent	30 percent

Over 85 percent of the radiation in this tabulation is estimated from the theory of references 11 and 31 to result from molecular band systems. A similar breakdown is indicated by the theory of references 5 and 8. (Ref. 8 was used to determine the total radiation levels above  $0.2\mu$ ; ref. 5, the broadband distributions. See preceding table.)

The broadband spectral analysis of radiation at the stagnation point for the Fire II experiment has been summarized graphically in figure 12. In that figure, the percentage of the radiation at wavelengths longer than  $0.2\mu$  that occurs above  $0.6\mu$  is plotted against the elapsed time from launch for the three experimental periods. The calculated points are the differences between the total radiometer and integrated spectral radiometer values divided by the total radiometer values. The numerator has been further adjusted to account for an estimate of the radiation in the  $0.2\mu$  to  $0.3\mu$  wavelength range during each data period. Although there appears to be fair agreement on spectral distribution between the Allen theory and the Fire results in each of the first two data periods, there does not appear to be as good agreement in the third data period where the molecular radiation predominates. The radiation for  $\lambda > 0.6\mu$  in the third data period estimated by the theory of references 11 and 31 results primarily from a relatively strong contribution of the  $N_2(1+)$  band system in the near infrared with a smaller contribution from the line radiation. The theory of references 5 and 8 indicates a smaller percentage contribution from the  $N_2(1+)$  band system and does not consider lines. If the small effect of line radiation is neglected, it would appear at least on the broadband level that the theoretical spectral distribution obtained from references 5 and 8 are in better agreement with the Fire II results for this third experimental period.

It is concluded therefore from the Fire II data that the spectral distribution of radiation intensity during the third data period becomes increasingly prominent in the  $0.3\mu$  to  $0.6\mu$  wavelength range, and appears to be fairly well predictable by the theories of references 5 and 8.

[REDACTED]

Total radiometer data analysis.- The results of the Fire II experiment for the two forebody total radiometers and the spectral radiometer are shown in figure 5. The reduced stagnation radiative heating rates ( $0.2\mu < \lambda < 4.0\mu$ ) are repeated in figure 6 and compared with the theories of Allen (refs. 11 and 31) and Nardone and Breene (ref. 8).

The Fire II total radiative heating rates are indicated in figure 5 to range from about  $31 \text{ W/cm}^2$  to  $22 \text{ W/cm}^2$  over this experimental period. The Fire I heating rates, by the nature of their reduction (see ref. 1), are more open to question as to their reliability. Calculations have indicated that selfabsorption in the plasma at wavelengths longer than  $0.2\mu$  was not significant at these flight conditions and thereby justifies the transparent gas analysis being used to determine the heating rates.

The Fire II results calculate to be a factor of about 1.6 below the theory of Allen at the beginning of the data period and increasing to about 2.4 at the end of that experiment. At these conditions, with line radiation neglected, the Breene and Nardone theory (ref. 8) is indicated to be in closer agreement with the Fire II data.

The effects of radiation cooling have been investigated in reference 27 in the same manner as that used for the second-data-period analysis. A value of the radiation-cooling factor equal to 0.99 was calculated for the  $\lambda > 0.2\mu$  wavelength range and this value indicated a negligible effect on the radiative heating. A similarly negligible effect was calculated for the entire wavelength range which included the potentially absorbing vacuum-ultraviolet radiation.

Forebody radiative heating distribution.- The offset radiometer in the Fire II third-data-period experiment indicated levels of radiation that were about 50 to 60 percent of the stagnation values. Interpolation between distributions for nominal preflight Fire trajectories in reference 30 indicates good agreement between that reference and the Fire results.

#### Additional Data Analysis

In figure 13 are indicated the complete record of the stagnation total radiometer and the integrations of the spectral radiometer data at the same location. An analysis of the data outside the prime data periods is made in appendix C. This analysis defines specific signal traces and anomalies in the radiometer record with respect to sequential events during the reentry. Some comparison is also made with the downrange optical coverage from Ascension Island which has been reported in references 32 and 33.

#### Ground-Facility Experimentation

Considerable ground-facility experimentation on hot-air radiation has been performed in recent years in shock tubes and ballistic ranges. Nerem (ref. 34) has compiled

[REDACTED]

[REDACTED]

the results of some of the more recent data on stagnation-point equilibrium air radiative emission. Those results obtained from references 18, 35, 36, and from a private communication between H. W. Ball of AEDC and Robert Nerem are for measurements of equilibrium air over a nominal wavelength range from  $0.2\mu$  to  $6.0\mu$  (the measurements of Nerem go to a lower wavelength limit of  $0.17\mu$ ). The data have been normalized by the stagnation density ratio to the 1.7 power and plotted against the simulated flight velocity. Nerem's compilation is shown in figure 14. Gruszczynski and Warren (ref. 28) conducted experiments on a hemispherical model ( $r_n = 2.54$  cm) in a shock tube which produced radiation intensities corresponding to a wide range of hyperbolic reentry velocities. Several measurements obtained in the simulated flight velocity range between 11 and 12 km/sec corresponded closely to the theoretical radiation levels for  $\lambda > 0.16\mu$  estimated by reference 8. The Gruszczynski and Warren data were total radiation measurements and did not imply any spectral distribution or species concentration. These data, solely on the basis of their correspondence to the reference 8 absolute radiation levels at those simulated velocities, suggest agreement with the Fire results for the condition of peak heating. The reference 28 data have been included in figure 14.

Other investigators have recently presented preliminary estimates (ref. 37) on the breakdown between the continuum and line radiation contributions of air at wavelengths longer than  $0.2\mu$  that were determined from curve fits of experimental data on similar breakdowns in nitrogen and oxygen. The facility used to make the measurements was a mechanically constricted, cascade direct-current arc. Their estimate of air radiation at  $\lambda > 0.2\mu$  (indicated by a dashed curve in fig. 14) favors the upper bound of ground-facility measurements in the flight velocity range of Project Fire. Of particular importance are the results of their distributions which indicate that approximately 70 percent of the radiation for  $\lambda > 0.2\mu$  at conditions corresponding to the first and second periods of the Fire experiments is the result of line radiation. In this respect, their estimated distribution of energy is in very good agreement with the results of the Fire II experiment, even though the absolute levels appear overestimated. Again, the effect of radiation cooling, which was not considered by these investigators, may produce a different result.

Also shown in figure 14 are the data for both Fire I and Fire II. The first data period of Fire I is not presented because of the strong nonequilibrium influence throughout that particular experiment and the attendant difficulty in determining a representative equilibrium zone thickness by which to reduce the heating rates to the volumetric units of figure 14. The Fire II first experimental period is indicated as a single point. This point was taken at the very end of that experiment ( $t = 1636.47$  sec) and is estimated to be representative of reasonably strong equilibrium contributions. As a result, the equilibrium zone thickness appears to be reasonably defined by the method of reference 1.

[REDACTED]

In general, the ground facility data are in agreement with the Project Fire results for the conditions of flight velocity corresponding to the first and second experimental periods. The results from the third data periods of both flights, however, indicate a trend lower than that exhibited by the ground facility results. At these velocities, the average level of radiation indicated by the ground facility data of figure 14 approximates the theoretical levels of Allen (refs. 11 and 31) calculated at the Fire conditions.

The general spread in the ground-facility points results primarily from the normalization of these data by the 1.7 power of the stagnation density. This rough approximation of the density dependence of radiation has been used by Nerem (ref. 34) and others to group the results of several investigators, results that were obtained by using a variety of testing mechanisms over a wide range of gas conditions. The velocity dependence of radiation indicated from such results is meaningful, in the broad sense, but the difficulty of making closer comparisons at discrete velocities is evident from the spread in the data in figure 14 which, at some velocities, approaches an order of magnitude.

#### Vacuum-Ultraviolet Radiation

In recent years, estimates have indicated that vacuum-ultraviolet radiation ( $\lambda < 0.2\mu$ ), although strongly self-absorbed, in many instances will provide a significant contribution to the radiative heating of vehicles entering the earth's atmosphere at lunar and interplanetary return velocities. This radiation, the result primarily of the de-ionization continua of nitrogen and oxygen ions and the atomic and ionic line bound-bound transitions, has been the stimulus of considerable theoretical work. Because of the inherent difficulties in obtaining measurements at these lower wavelengths, little experimental data are available. The Project Fire experiment has yielded results that can be analyzed in a manner that, although implicit in nature, can roughly account for the radiation contribution in the vacuum-ultraviolet spectrum. These flight results and their assessment in light of the current theory are discussed in this section.

Calorimeter heating rates and associated analysis.- The stagnation total heating rates for the Fire II experiment, which were obtained from reference 12, are shown in figure 15. These heating rates, which were determined from the temperature-time histories of the forebody calorimeters, indicate the contributions from the convective and absorbed radiative heating components at the calorimeter surface. By using these total heating rates and the measured radiative heating rates for the energy above  $0.2\mu$  along with the calorimeter surface absorptivity properties shown in figure 3, an estimate of the radiation from the vacuum-ultraviolet sources can be inferred.

In analyzing the vacuum-ultraviolet radiation, the convective heating rates throughout the reentry were assumed to be known. In this analysis, the method of reference 38 was used to adjust the convective heating levels calculated by the theory of reference 39

[REDACTED]



[REDACTED]

in order to account for deviations from Newtonian theory. These values conformed well with levels obtained from other representative theories for flight velocities up to 12 km/sec. On that basis and the fact that good correspondence was indicated with the Fire II third-data-period results where, at the lower velocities, the convective heating was dominant, it was assumed that, in the absence of radiative and convective coupling, reasonably accurate estimates of convective heating could be assured by using the adjusted Cohen theory. The coupling effect, which normally results in a lower enthalpy difference across the boundary layer, serves to lower the convective heating rate.

In the first data period, the early cut-off of the radiation experiment inhibits any meaningful analysis on vacuum-ultraviolet radiation. Nonequilibrium effects further complicate the analysis at these early reentry times. The radiative heating experienced in the third data period was extremely low compared with the convective heating and thus precluded any significant vacuum-ultraviolet analysis at those times. The prime analysis of the vacuum-ultraviolet radiation, therefore, has been restricted to the second-data-period experiment. To the calculated stagnation convective heating rates (short-dashed curve in fig. 15) were added the measured radiative heating rates deduced from the total radiometer experiment. These radiative rates were adjusted by a spectrally weighted value of absorptance at  $\lambda > 0.2\mu$  for the calorimeter which for the second data period was estimated to be 0.52. The sum of the heating rates from the absorbed radiation above  $0.2\mu$  and the calculated convective component were then subtracted from the calorimeter total heating rates. The difference was estimated to represent the absorbed vacuum-ultraviolet radiation.

The remaining step in this phase of the analysis was to determine an effective value of calorimeter absorptance in the wavelength region,  $\lambda < 0.2\mu$ , from which to deduce a final level of vacuum-ultraviolet radiation. Once again, a spectrally weighted estimate of absorptance for the calorimeter based on the line and continuum contributions of reference 11 was used in conjunction with the calorimeter absorptance distribution shown in figure 3. A substitution of the values shown in columns (35) and (36) of table I into the following equation

$$\alpha_{\text{mean}} = \frac{(\dot{q}_{\text{al}})\alpha_{\text{al}} + (\dot{q}_{\text{cont}})\alpha_{\text{cont}}}{\dot{q}_{\text{al}} + \dot{q}_{\text{cont}}} \quad (\lambda < 0.2\mu)$$

yielded a value of  $\alpha_{\text{mean}}$  equal to 0.89.

The absorbed vacuum-ultraviolet radiation obtained from figure 14 at approximately the midtime of the second data period (1642.65 sec) was calculated to be  $140 \text{ W/cm}^2$ . The correction for calorimeter absorptance yielded a value of  $157 \text{ W/cm}^2$ , which represents the stagnation radiative heating rate from the vacuum-ultraviolet sources inferred from

Fire II flight measurements. (The measured radiative heating rate for  $\lambda > 0.2\mu$  at this representative time was approximately 330 W/cm<sup>2</sup>.)

Comparison of vacuum-ultraviolet theory with the Fire II calculations.- A theoretical estimate of the Fire II stagnation radiative heating rates from vacuum-ultraviolet contributions based on reference 11 are presented in columns (22) and (23) of table I. An interpolation of the tables at the representative time under consideration (1642.65 sec) yielded values of  $\dot{q}_{al} = 278$  W/cm<sup>2</sup> and  $\dot{q}_{cont} = 137$  W/cm<sup>2</sup> for a total of 415 W/cm<sup>2</sup>. On this basis of comparison, the theory overpredicts the vacuum-ultraviolet radiative heating rate calculated from the Fire II experiment by a factor of about 2.6.

Olstad's analysis (ref. 27)\* at the second-data-period conditions indicated that in the vacuum-ultraviolet spectrum ( $\lambda < 0.2\mu$ ), the value of stagnation radiative heating for the nonisothermal, absorbing gas calculation was approximately 0.57 that for the isothermal absorbing-gas case, which was the basis of the reference 11 theory. The associated coupling effect reduced the convective heating rate to 0.93 of the value calculated with the Cohen theory.

With the use of Olstad's results and the method of calculation previously described in figure 15, the absorbed stagnation vacuum-ultraviolet radiative heating rate was shown to increase from 140 W/cm<sup>2</sup> to 187 W/cm<sup>2</sup> as a result of the decrease in the convective heating component due to coupling. Upon adjusting for calorimeter absorptance, the vacuum-ultraviolet radiative heating rate was calculated to be 210 W/cm<sup>2</sup>. The theoretical estimate of 415 W/cm<sup>2</sup>, when adjusted by the radiation-cooling factor of 0.57, was reduced to 236 W/cm<sup>2</sup>. The radiative heating rate for  $\lambda < 4.0\mu$  was indicated therefore from the Fire II experiment (at  $t = 1642.65$  seconds) to be about 540 W/cm<sup>2</sup>.

In figure 16 are indicated the comparisons between the vacuum-ultraviolet radiation theory and the results inferred from the Fire measurements with and without a consideration of radiation cooling and coupling. The importance of allowing for these effects is very vividly demonstrated. The radiation cooling and coupling analysis conducted by Olstad, when applied to the Allen theory at the Fire II second-data-period flight conditions, indicated levels of vacuum-ultraviolet radiative heating that were in good agreement with the levels deduced from the Fire II calorimeter and radiometer measurements and the Cohen convective heating theory. It is concluded therefore from these Fire II results that analyses which do not include a consideration of cooling and coupling effects may be prone to considerable error.

---

\*Because of the slight differences in calorimeter absorptance values and the difficulty in obtaining similar absolute intensity values from the referenced theories, some differences were noted in the values shown in this report and those calculated by Olstad. To minimize the effect of these differences, the data obtained from Olstad's work have been extracted solely in the form of ratios and factors, or otherwise normalized values.

## Total Heating Theory and the Fire II Results

In figure 15 are indicated by a solid heavy line the measured Fire II calorimeter heating rates for the three data periods. The details of the determination of these heating rates from the calorimeter data are covered in reference 12. A theory of total heating is also shown in figure 15 by a long-dashed line. It is composed of estimates based on the equilibrium radiation theory of Allen (refs. 11 and 31), the empirical non-equilibrium radiative heating of Page and Arnold (ref. 18), and the convective heating theory of Cohen (ref. 39), adjusted for Newtonian assumptions by the method of Boison and Curtiss (ref. 38). The composite theory gives heating rates that are in general higher than those indicated by the Fire II experiments in both the first and second data periods. There is very good agreement between the theory and the Fire II results in the third data period owing principally to the dominating influence of convective heating during that experiment. The Fire results, in fact, would appear to offer strong testimony to the accuracy of the stagnation-point convective heating theory of reference 39 at flight velocities below 9 km/sec.

In view of the relatively low radiative heating rates exhibited during the first data period, the poor agreement between the composite theory and the Fire II results would appear to result from unrealistic theoretical estimates of convective heating at these early reentry conditions. The Fire II results are between 10 to 30 percent lower than the composite theory. These lower convective heating rates appear to contradict the theory for low Reynolds number effects. (See ref. 40.) Because of the contrary evidence, however, indicated by the Fire I experiment (refs. 1 and 2), which shows the Fire results to be higher than the convective heating theory, no positive conclusions on total heating can be made for the first-data-period experiment. It does appear, however, that the use of boundary-layer theory to estimate convective heating at these early reentry conditions must be tempered with other theoretical considerations.

The differences between the composite heating theory and the Fire II calorimeter heating rates during the second data period have been analyzed in much of the previous discussion. Radiation cooling and coupling between the radiative and convective modes of heating appear to account largely for the differences shown. Support for this conclusion is evidenced further by the shift in the peak of the total heating pulse indicated by the calorimeter heating rates. A theoretical calculation of total heating without radiation cooling or coupling for a reentry-type trajectory generally undergoes a peak shift to a later time when cooling and coupling adjustments are made. In figure 15 is indicated at the representative time of 1642.65 seconds a theoretical estimate of total heating rate of  $1034 \text{ W/cm}^2$ . This value was calculated by applying the radiation-cooling and coupling effects estimated by Olstad (ref. 27) to the composite heating rate indicated in the figure and in column (38) of table I. This estimate is in good agreement with the Fire II results at that time.

## CONCLUSIONS

During three discrete experimental periods, direct measurements of gas radiation at wavelengths greater than  $0.2\mu$  were obtained from the onboard radiometers of the Fire II reentry package. The conclusions that follow are based primarily on comparisons between the measured radiation levels and the theory.

1. With a consideration of existing ground-facility experimental data, the information provided by the Fire I and Fire II radiative heating results during early reentry indicated the possibility of a greater velocity dependence of nonequilibrium radiative heating than that indicated by an early fairing of ground-facility data. At the Fire entry velocities (slightly greater than 11 km/sec), a ninth-power dependence appears to be more realistic than the previously indicated fourth-power dependence.

2. The truncation effect at the conditions associated with the ballistic entry of the blunt Fire body appears to be predictable by available methods. Other radiation-limiting effects during early reentry appear to be reasonably predictable by the "collision-limiting" relationship developed in this report.

3. The results for the early reentry and peak heating conditions of the Fire II experiment and the early heating conditions of the Fire I experiment indicate that about three-quarters of the incident stagnation radiation at wavelengths longer than  $0.2\mu$  occurs above  $0.6\mu$ , and suggests strong contributions from atomic lines.

4. The analysis near peak heating indicated that at the conditions of flight associated with that Fire II experiment, the radiative heating in the wavelength ranges,  $\lambda > 0.2\mu$  and  $\lambda < 0.2\mu$ , is closely predictable by the theory of Allen adjusted to account for radiation cooling as calculated by the method of Olstad.

5. The total stagnation heating rates measured near peak heating by the Fire calorimeters appear to be reasonably predictable at these flight conditions by the equilibrium radiation estimates of Allen, the empirical nonequilibrium radiation heating of Page and Arnold, and the convective heating of Cohen, the combined theories adjusted for radiation cooling and coupling effects as indicated by Olstad.

6. The data from the Fire II experiment at conditions of reduced velocity and relatively high density indicate that the molecular theory of Breene and Nardone are in close agreement with the Fire results at these conditions.

Langley Research Center,

National Aeronautics and Space Administration,

Langley Station, Hampton, Va., December 6, 1966,

714-00-00-01-23.

## APPENDIX A

### CORRECTIONS TO RADIOMETER DATA

An unavoidable shortcoming of the calibration procedure for the Project Fire total radiometers was the impossibility of duplicating in the laboratory the spectral distribution of the gas radiance to which the instruments would be subjected in flight. In this appendix are discussed the methods by which correction factors for the radiometer data for both Fire I and Fire II were determined. These corrections were based on the instrument calibration procedures and the optical elements of the radiometers and calibration setup.

When the Fire I radiometer data were reduced (ref. 1), the optics used in the flight instruments and laboratory calibration setup were assumed to be gray (that is, exhibiting constant spectral response over the applicable wavelength range,  $0.2\mu < \lambda < 4.0\mu$ ). The Fire II steradiancy levels  $I_r$  from the original telemetry records (fig. 4) were obtained by using these same assumptions. Deviations from such spectral flatness that were recognized on the basis of commercial values of optical properties were used to estimate limits of precision for the Fire I data. (See appendix A of ref. 1.) Recent measurements on similar radiometer components (spare units) have resulted in what is estimated to be more reliable values of optical properties for the flight components. Measurements have similarly been made of the properties of the components of the calibration setup. This postflight information is used in this appendix to determine correction factors by which to adjust the Fire I data.

The measurements described, except for minor changes arising from the use of different optics in the calibration setup, were also used to reduce the Fire II data presented in this report. A detailed description of the procedures used is given in reference 41.

#### Stagnation Radiometer

The spectral distribution used in the calibration procedure resulted from the combined contributions of a heated carbon block source and the quartz optics (furnace window and focusing lenses) used to image the block at the intensity-measuring thermocouple. This lampblack thermocouple and the metal screen filters used in the Fire I calibration were assumed to be spectrally flat. It was also assumed that the carbon block emitted as a gray body with an emissivity of 0.9. The reflectance of the  $MgF_2$ -coated aluminized beam splitter and the transmittance of the double lens for the stagnation radiometer were obtained from laboratory measurements. The gold black instrument thermopiles when

## APPENDIX A

calibrated relative to the calibration thermocouple indicated but small differences in response and were therefore assumed to be gray.

The calibration of the Fire II radiometer differed in that inconel neutral density filters were used instead of the metal screens in the Fire I calibration setup. The spectral transmittance of these inconel filters was considered in determining the spectral shape of the calibration source for the Fire II instrument calibration.

The instrument response to the laboratory calibration source may be determined from the following relationship:

$$R_{cal} = \frac{\int_{0.2\mu}^{4.0\mu} B_{\lambda} T_{\lambda} F_{\lambda} L_{\lambda} R_{\lambda} d\lambda}{\int_{0.2\mu}^{4.0\mu} B_{\lambda} T_{\lambda} F_{\lambda} d\lambda} \quad (A1)$$

where the terms of the equation representing, in part, the optical properties of the various components of the radiometer and calibration systems are defined in the list of symbols. The term  $F_{\lambda}$  representing the filter transmittance associated with the Fire II calibration procedure was considered to be constant in determining the Fire I calibration response and therefore did not affect the value of  $R_{cal}$  calculated for that calibration.

In order to determine the radiometer response during the flight experiments, it was necessary to estimate spectral distributions from the shocked air source in front of the Fire body. Instrument response during reentry is given by

$$R_{flt} = \frac{\int_{0.2\mu}^{4.0\mu} I_{\lambda} \tau_{\lambda}^N L_{\lambda} R_{\lambda} d\lambda}{\int_{0.2\mu}^{4.0\mu} I_{\lambda} \tau_{\lambda}^N d\lambda} \quad (A2)$$

where  $I_{\lambda}$  represents the estimated spectral distribution of gas radiance and  $\tau_{\lambda}^N$  the transmission of the quartz window array. (The exponent  $N$  denotes the number of windows through which the radiation was viewed at any particular time.) Molecular and continuum radiative heating estimates for the first and second data periods were calculated from the absorption coefficients of reference 7. These estimates were supplemented by estimates of line radiation obtained from reference 11. Reference 31 was used for the strong molecular contributions in the third data period. Nonequilibrium radiation estimates were obtained from references 17 and 18.

## APPENDIX A

As a result of the postflight analysis, therefore, the Fire I stagnation radiometer data and calculated radiative heating rates presented in reference 1 must be adjusted by using the following equation:

$$\text{Corrected Fire I data} = (\text{Fire I data of ref. 1}) \left( R_{\text{cal}} / R_{\text{flt}} \right) \quad (\text{A3})$$

where the ratio  $R_{\text{cal}} / R_{\text{flt}}$  is the correction necessary to account for the change in instrument response during the flight experiment from that exhibited during the laboratory calibration. Following are tabulated the values of  $R_{\text{cal}} / R_{\text{flt}}$  that were used to adjust the Fire I stagnation data and heating rates in reference 1:

Data period	$R_{\text{cal}} / R_{\text{flt}}$
First	1.404
Second	1.398
Third	1.540

The initial steradiancy levels  $I_r''$  for Fire II which are indicated in figure 4 must be similarly adjusted to account for the optical behavior of the radiometer. The corrections may be determined by

$$I_r' = I_r'' \frac{R_{\text{cal}}}{R_{\text{flt}}} \quad (\text{A4})$$

The resulting Fire II factors for the stagnation radiometer were

Data period	$R_{\text{cal}} / R_{\text{flt}}$
First	1.295
Second	1.256
Third	1.400

### Offset and Afterbody Radiometers

The total radiometers positioned at the offset and afterbody locations were calibrated in the laboratory by using the same procedure as that for the stagnation instrument. These radiometers differed in construction, however, in that an aluminum mirror rather than a beam splitter served as the internal reflecting element and the acceptance lens was a single element instead of the double lens used in the stagnation instrument.

## APPENDIX A

Because of the body motions experienced during the second and third data periods of the Fire I reentry, the radiation data obtained by the offset and afterbody radiometers at those times were considered to be unreliable. During the first data period, however, prior to the onset of the motions, the Fire I records were good and the data were reported in reference 1. The estimated spectral distribution  $I_\lambda$  for determining  $R_{flt}$  at the offset location was assumed to be the same as that for the stagnation region. A correction factor of  $R_{cal}/R_{flt}$  equal to 1.077 was calculated for the offset radiometer data and heating rates for the first data period of Fire I.

The factors by which the indicated offset radiometer steradiancies for the Fire II experiment must be corrected are

Data period	$R_{cal}/R_{flt}$
First	1.023
Second	1.016
Third	1.072

Because of the difficulty in estimating a spectral distribution suitable for the afterbody radiometer during reentry, no correction factor was considered for those radiation data for either flight. In the afterbody region of the flow field, the temperature of the plasma is significantly reduced and has been estimated (refs. 23, 24, and 29) to be around 3000° K. Because of these low temperatures which more nearly approach the level of the source used for the instrument calibration (2500° K), and because of the smaller resulting correction factors for the instruments with aluminum mirrors, the afterbody data were not considered to require correction.



## APPENDIX B

### FIRE II ERROR ANALYSIS

The accuracy of the Fire II radiative heating rates presented in this report was calculated by using the same maximum deviation approach that was employed in reference 1 for the Fire I results. Three principal sources of error were investigated:

- (1) Radiometer calibration
  - (a) Spectral response of components of instrument and calibration setup
  - (b) Estimate of spectral distribution of gas steradiancy for the flight experiment
- (2) Flight telemetry error
- (3) Readability of reduced data

#### Radiometer Calibration

A detailed postflight analysis was made to determine the maximum deviations attributable to item 1(a) for the four flight instruments (three total and one spectral radiometer). The details of this study are reported in reference 41. It was concluded in that report that the following deviations were applicable to the flight instruments:

All total radiometers . . . . .	±10 percent
Spectral radiometer . . . . .	±20 percent

A maximum deviation of ±10 percent was assumed for item 1(b) for the three total radiometers in all three data periods. This value appeared to reflect adequately the differences that still may be inferred from the various theoretical spectral distributions. The value of  $R_{\text{fl}t}$  in equation (A2) is, in any event, fairly insensitive to this assumed value of absolute intensity  $I_{\lambda}$ . For the spectral radiometer, item 1(b) does not apply inasmuch as there is essentially no averaging of spectral distribution necessary over its narrow  $0.002\mu$  instrument bandpass.

#### Flight Telemetry Error

This section deals solely with the accuracy of the flight telemetry system. The system was estimated to be accurate within ±2 percent of voltage reading for the total and spectral radiometer data. This deviation for the telemetry bandwidth corresponding to 5 volts full scale indicated that the data recorded at ground receiving stations were accurate to within ±0.1 volt. The maximum deviations in intensity level tabulated below were estimated from the voltage variations indicated by the instrument calibration curves:

## APPENDIX B

Instrument	First data period	Second data period	Third data period
Stagnation total	±10 percent	±15 percent	±10 percent
Offset total	±10 percent	±20 percent	±20 percent
Stagnation spectral	±10 percent	±10 percent	±10 percent

### Readability of Reduced Data

The estimated errors for item (3) for the total radiometers reflect the degree to which the raw data signal was interpretable from the standpoint of both the telemetry noise and the fairing procedure used to compensate for the body motions. On a percent-age basis, each problem appeared to have about an equal effect estimated to be about ±5 percent for the stagnation instrument. The fairing procedure used with respect to the offset radiometer data in the second and third data period is subject to more error. As a result, the maximum item (3) deviations for the offset radiometer in those periods have been estimated to be ±20 percent.

The noise in the telemetry system was approximately the same for the spectral radiometer record as that for the total radiometers. Because of the unique significance, however, of each point on the spectral radiometer record, the fairing method used to reduce the total radiometer records during the second and third data periods did not apply for this instrument. The body motions, on the other hand, affected the readability of the spectral records in a different way. The finite time interval needed to cover a single spectral scan (about 0.075 second) was of the order of the period of a single sinusoidal-like body motion. Each scan, therefore, consisted of measurements taken over a varying angle of attack. The maximum angles of attack for the second and third data periods were approximately 5° and 10°, respectively. On the basis of the intensity distribution at the geometrical stagnation point at angle-of-attack conditions shown in reference 1, it was assumed that representative values of  $(\dot{q}_{r,\alpha}/\dot{q}_{r,\alpha=0})_{s/s_c=0}$  equal to 0.97 and 0.93 should apply, respectively, to the second- and third-experimental-period data and subsequent integrations.

Values of the maximum deviations for item (3) which resulted from this analysis of the total and spectral radiometers are summarized in the following table:

Instrument	First data period	Second data period	Third data period
Stagnation total	±10 percent	±10 percent	±10 percent
Offset total	±10 percent	±20 percent	±20 percent
Stagnation spectral	±5 percent	+8 percent -5 percent	+12 percent -5 percent

## APPENDIX B

The final maximum deviation values for all three items for the two forebody total radiometers and the spectral radiometer are shown in the following table:

Instrument	First data period	Second data period	Third data period
Stagnation total	+46 percent -34 percent	+53 percent -38 percent	+46 percent -34 percent
Offset total	+46 percent -34 percent	+74 percent -48 percent	+74 percent -48 percent
Stagnation spectral	+39 percent -32 percent	+43 percent -32 percent	+48 percent -32 percent

A more representative assessment of the accuracies of the various instruments may be indicated by the root-sum-square (rss) deviation defined by the following equation:

$$\sigma(\text{rss}) = \sqrt{(\sigma_{1a})^2 + (\sigma_{1b})^2 + (\sigma_2)^2 + (\sigma_3)^2} \quad (\text{B1})$$

where the subscripts denote the source of the error.

The resulting root-sum-square deviations are tabulated below:

Instrument	First data period	Second data period	Third data period
Stagnation total	±20 percent	±23 percent	±20 percent
Offset total	±20 percent	±32 percent	±32 percent
Stagnation spectral	±23 percent	+24 percent -23 percent	+25 percent -23 percent

## APPENDIX C

### DATA ANALYSIS OUTSIDE PRIME DATA PERIODS

In figure 13 are indicated the complete record of the stagnation total radiometer ( $0.2\mu < \lambda < 4.0\mu$ ) and the integrations of the spectral radiometer data at the same location. The wavelength ranges for the forward and reverse scans of the spectral instrument are repeated below:

Forward scan:  $0.3\mu < \lambda < 0.5575\mu$

Reverse scan:  $0.3\mu < \lambda < 0.609\mu$

All radiation has been reduced to units of watts/centimeter<sup>2</sup>-steradian and represents the steradiance levels in the plasma incident at the stagnation point of the reentry package. A reduction to steradiancy units is necessary in making the type of analysis intended here. In particular, geometry factors for the plasma must be excluded in dealing in a composite fashion with a radiating clean transparent air plasma, absorbing ablation products, and glowing forward windows.

The total radiometer levels  $I_T$  indicated in figure 13 have been adjusted for the instrument calibration correction (appendix A) and window transmission. In these respects, they represent a transcription from the fairing made through the raw data shown in figure 4. For those regions of the record outside the three primary data periods, no calibration correction could be made. In the absence of any definable spectral distribution for the ablation products and/or window radiation, the assumption was made that such emission would reasonably approximate that of the infrared instrument calibration source, and thus obviate any such correction.

The dashed portions of the total radiometer record and the blackened spectral radiometer symbols indicate the data obtained during the three primary experimental periods. These periods covered times when clean calorimeters were exposed and the temperature of the outer surface of the quartz window in the exposed calorimeter was calculated to be still below the melting point. These experimental period data, reduced to heating rates, are also shown in figure 5. The total radiometer record in figure 13 also embodies a fairing through certain regions of the record where the low-amplitude high-frequency body motions were prominent; the initial data record shown in figure 4 for the three total radiometers indicates all the motions. The discussion that follows covers chronologically the sequence of significant events affecting the interpretation of the radiometer records in figures 4 and 13.

## APPENDIX C

1636.47 seconds: The quartz window in the first calorimeter was estimated to have reached surface melt; thereby, the termination of the radiation experiment for the first data period was signaled.

1636.47 to 1642.47 seconds: During this period, the forward quartz window continued to deteriorate. The radiation from a glowing window would not be expected to produce much more than 5 to 10 percent of the measured radiation levels at these times. This result, coupled with the absence of any abrupt changes in signal between 1636.47 and 1639 seconds, tends to imply a condition of partial transparency for the exterior window through that period of time.

The stagnation calorimeter reached surface melt at approximately 1639.92 seconds. (See ref. 12.) The onset of the body motions occurred at 1640.35 seconds. These two events both correspond very closely to a strong "blackout" of signal on both the stagnation and offset radiometers at 1640.44 seconds. It is estimated that the three events (calorimeter melt, body motions, and signal "blackout") are closely related; that is, the body motions may well have resulted from unsymmetrical melting of the beryllium calorimeter. The radiation "blackout" (which occurred on both the total and spectral radiometers at the stagnation point) could have resulted from the flowing beryllium. This theory is supported to a degree by the slight enhancement of signal on the afterbody radiometer.

During the period prior to "instrument blackout," the integrated spectral radiometer radiation may be observed to have decreased with increasing time whereas the stagnation total radiometer signal continued to increase during this same period. This condition suggested a shift in source radiance to the infrared wavelengths which indicated the possibility of the presence of radiation from either ablation products or the deteriorating windows. It was not possible to determine when the window in the first phenolic asbestos heat shield became exposed, but it might have occurred at the time indicated by signal recovery (1641.30 sec).

The body motions during these times were of a coning nature exhibiting maximum angles of attack of approximately  $5^{\circ}$ .

1642.47 to 1642.90 seconds: Second data period (see appropriate section in report). The signal indicating the actual heat-shield ejection may be seen in figures 4 and 13. The stagnation and offset radiometer records indicated sharp drops in signal as the shields slid away and passed the windows. The afterbody record indicated a slight enhancement of signal (fig. 4) immediately afterward; this response is one of the few recorded by the insensitive afterbody radiometer.

1642.90 to 1648.16 seconds: The body motions continued at about the same magnitude and still exhibited a coning action. The second calorimeter reached surface melt

## APPENDIX C

between 1645.0 and 1645.3 seconds. A slight disturbance may be noted on figures 4 and 13 at the later time but no appreciable changes in body motions resulted in this instance. The offset radiometer signal, however, deteriorated considerably at this point and remained so for the next 2 seconds. (See fig. 4.)

At 1646.2 seconds the stagnation total radiometer traced out a "hump" lasting about 1 second. It is felt that the signal enhancement indicated here corresponded to the exposure of the second phenolic heat-shield window. The expected increase in transmission and the more clear definition of the body motions tend to substantiate this premise. A sizable drop in the stagnation total radiometer signal of about 0.1-second duration occurred midway in the "hump." This drop may have resulted from some momentary contamination on the window.

At approximately 1647.54 seconds occurred what was probably the brightest flash observed from the downrange ground stations during the entire reentry. (See refs. 32 and 33 for a complete analysis of the optical ground coverage.) It was recorded as well on all four onboard radiometers. In reference 32, the flash was identified as the flaring up and burning off of a segment of beryllium. This result is substantiated by the data reported in reference 33 which indicate BeO to be the prime radiator at this instant.

1648.16 to 1648.50 seconds: Third data period (see appropriate section in report). The heat-shield ejection is indicated rather clearly by a drop in signal on the offset radiometer trace and verified on the afterbody radiometer record immediately afterward. (See fig. 4.)

1648.50 to 1652.0 seconds: Throughout most of this period, the spectral radiometer integrations are indicated to contribute about 50 percent of the amount of radiation indicated by the total radiometer. At the beginning of this interval, a "hump" similar in nature to that observed at 1647 seconds would tend to indicate a possible loss of window in the third beryllium calorimeter. However, the calorimeter itself was estimated to have remained intact until about 1653 seconds, individual sections surviving through the remainder of the reentry (ref. 13). It was primarily because of this anomaly that the third-data-period analysis was shortened to one-half the estimated window lifetime.



## REFERENCES

1. Cauchon, Dona L.: Project Fire Flight 1 Radiative Heating Experiment. NASA TM X-1222, 1966.
2. Cornette, Elden S.: Forebody Temperatures and Total Heating Rates Measured During Project Fire 1 Reentry at 38 000 Feet Per Second. NASA TM X-1120, 1965.
3. Slocumb, Travis H., Jr.: Project Fire Flight 1 Heating and Pressure Measurements on the Reentry-Vehicle Afterbody at a Velocity of 38 000 Feet Per Second. NASA TM X-1178, 1965.
4. Scallion, William I.; and Lewis, John H., Jr.: Flight Parameters and Vehicle Performance for Project Fire Flight 1, Launched April 14, 1964. NASA TN D-2996, 1965.
5. Breene, R. G., Jr.; and Nardone, Maria: Radiant Emission From High Temperature Equilibrium Air. R61SD020 (Contract No. AF 04(647)249), Space Sci. Laboratory, General Electric Co., May 1961.
6. Kivel, B.; and Bailey, K.: Tables of Radiation From High Temperature Air. Res. Rept. 21 (Contracts AF 04(645)-18 and AF 49(638)-61), AVCO Res. Lab., Dec. 1957.
7. Meyerott, R. E.; Sokoloff, J.; and Nicholls, R. A.: Absorption Coefficients of Air. AFCRC-TR-59-296, U.S. Air Force, Sept. 1959.
8. Nardone, M. C.; Breene, R. G.; Zeldin, S. S.; and Riethof, T. R.: Radiance of Species in High Temperature Air. Tech. Inform. Ser. R63SD3 (Contract AF 04(694)-222), Missile and Space Div., Gen. Elec. Co., June 1963. (Available From DDC as AD No. 408564.)
9. Hahne, Gerhard E.: The Vacuum Ultraviolet Radiation From  $N^{+}$ - and  $O^{+}$ -Electron Recombination in High-Temperature Air. NASA TN D-2794, 1965.
10. Biberman, L. M.; Iakubov, I. T.; Norman, G. E.; and Vorobyov, V. S.: Radiation Heating Under Hypersonic Flow. Astronaut. Acta, vol. X, fasc. 3-4, 1964, pp. 238-252.
11. Allen, Richard A.: Air Radiation Graphs: Spectrally Integrated Fluxes Including Line Contributions and Self Absorption. Res. Rept. 230, Avco-Everett Res. Lab., Sept. 1965.
12. Cornette, E. S.: Forebody Temperatures and Calorimeter Heating Rates Measured During Project Fire II Reentry at 11.35 Kilometers Per Second. NASA TM X-1305, 1966.

- [REDACTED]
13. Dingeldein, Richard C.: Radiation and Total Heating Rates Obtained From Project Fire Reentries at 37,000 Feet Per Second. NASA paper presented at AFFDL/ASSET Advanced Lifting Reentry Technology Symposium (Miami Beach, Fla.), Dec. 14-16, 1965.
  14. Slocumb, Travis H., Jr.: Project Fire Flight II Afterbody Temperatures and Pressures at 11.35 Kilometers per Second (37 200 Feet per Second). NASA TM X-1319, 1966.
  15. Scallion, W. I.; and Lewis, John H., Jr.: Flight Parameters and Vehicle Performance For Project Fire Flight II. NASA TN D-3569, 1966.
  16. Woodbury, Gerard E.: Angle-of-Attack Analysis for Project Fire 1 Payload Reentry Flight. NASA TN D-3366, 1966.
  17. Allen, R. A.; Rose, P. H.; and Camm, J. C.: Non-Equilibrium and Equilibrium Radiation at Super-Satellite Re-Entry Velocities. Paper No. 63-77, Inst. Aerospace Sci., Jan. 1963.
  18. Page, William A.; and Arnold, James O.: Shock-Layer Radiation of Blunt Bodies at Reentry Velocities. NASA TR R-193, 1964.
  19. Hoshizaki, H.; and Wilson, K. H.: Convective and Radiative Heat Transfer During Superorbital Reentry. AIAA Paper No. 66-106, Am. Inst. Aeron. Astronaut., Jan. 1966.
  20. Camm, J. C.; Kivel, B.; Taylor, R. L.; and Teare, J. D.: Absolute Intensity of Non-Equilibrium Radiation in Air and Stagnation Heating at High Altitudes. J. Quant. Spectry. & Radiative Transfer, vol. 1, no. 1, Sept. 1961, pp. 53-75.
  21. Teare, J. D.; Georgiev, S.; and Allen, R. A.: Radiation From the Non-Equilibrium Shock Front. Res. Rep. 112 (AFCRL 937), Avco-Everett Res. Lab., Oct. 1961.
  22. Canning, Thomas N.; and Page, William A.: Measurements of Radiation From the Flow Fields of Bodies Flying at Speeds Up to 13.4 Kilometers Per Second. Presented to the Fluid Mechanics Panel of AGARD (Brussels, Belgium), Apr. 3-6, 1962.
  23. Vinokur, M.; Nicolet, W. E.; Buckingham, A. C.; and Hoshizaki, H.: Project Fire - Flow Field Prediction and Analysis. M-12-65-1 (NASA CR-63401), Lockheed Missiles & Space Co., Mar. 1965.
  24. Kuby, W. C.; Byron, S. R.; Foster, R. M.; Hoglund, R. F.; and Holt, M.: Analysis of the Project Fire Re-Entry Package Flow Field. Publ. No. U-3020 (NASA CR-63388), Aeronutronic Div., Philco Corp., Oct. 8, 1964.
- [REDACTED]



- [REDACTED]
25. Howe, John T.; and Viegas, John R.: Solutions of the Ionized Radiating Shock Layer, Including Reabsorption and Foreign Species Effects, and Stagnation Region Heat Transfer. NASA TR R-159, 1963.
  26. Goulard, R.: The Coupling of Radiation and Convection in Detached Shock Layers. J. Quant. Spectrosc. Radiat. Transfer, vol. 1, Pergamon Press Ltd., 1961, pp. 249-257.
  27. Olstad, W. B.: Prediction of the Stagnation-Point Radiation Heat Transfer for the Project Fire Reentry Vehicle. NASA TM X-1401, 1967.
  28. Gruszczynski, J. S.; and Warren, W. R., Jr.: Study of Equilibrium Air Total Radiation. AIAA Paper No. 66-103, Jan. 1966.
  29. Brunner, M. J.; Dohner, C. V.; Langelo, V. A.; and Rie, H.: Flow Field Prediction and Analysis - Project Fire. Doc. No. 64SD727 (NASA CR-60451), Re-Entry Syst. Dept., Gen. Elec. Co., May 29, 1964.
  30. Stainback, P. Calvin: Convective and Equilibrium Radiation Heat-Transfer Predictions for Project Fire Reentry Vehicle. NASA TN D-2867, 1965.
  31. Allen, R. A.: Air Radiation Tables: Spectral Distribution Functions for Molecular Band Systems. Res. Rept. 236 (Contracts NASw-748 and DA-01-021-AMC-12005(2)), Avco-Everett Research Lab., Apr. 1966.
  32. McKee, Charles W.: Project Fire Photographic Summary and Record of Reentry Phenomena at Hyperbolic Velocities. NASA TN D-3571, 1966.
  33. Signature Processing: Optical Signature Data Report 65-020 for Test 0501 (Project Fire). Vols. I-III, RCA Serv. Co., A.F. Eastern Test Range, Nov. 5, 1965.
  34. Nerem, Robert M.: Radiating Flows Around Re-Entry Bodies. Presented at the XVIth International Astronautical Congress (Athens, Greece), Sept. 1965.
  35. Nerem, Robert M.; and Stickford, George H.: Shock Layer Radiation During Hypervelocity Re-Entry. AIAA Entry Technology Conference, CP-9, Am. Inst. Aeron. Astronaut., Oct. 1964, pp. 158-169.
  36. Hoshizaki, Hiroshi: Equilibrium Total Radiation Measurements in Air at Superorbital Entry Velocities. Third Hypervelocity Techniques Symposium, Univ. of Denver and Arnold Eng. Develop. Center, Mar. 1964, pp. 245-281.
  37. Morris, J. C.; Knopp, C. F.; Krey, R. U.; Liebermann, R. W.; and Garrison, R. L.: Radiation of Oxygen and Nitrogen and Thermal Conductivity of Nitrogen Up to 15,000° K. Paper No. 66-182, Am. Inst. Aeron. Astronaut., Mar. 1966.


- 
38. Boison, J. Christopher; and Curtiss, Howard A.: An Experimental Investigation of Blunt Body Stagnation Point Velocity Gradient. ARS J., vol. 29, no. 2, Feb. 1959, pp. 130-135.
39. Cohen, Nathaniel B.: Boundary-Layer Similar Solutions and Correlation Equations for Laminar Heat-Transfer Distribution in Equilibrium Air at Velocities Up to 41,100 Feet Per Second. NASA TR R-118, 1961.
40. Howe, John T.; and Sheaffer, Yvonne S.: Mass Addition in the Stagnation Region for Velocity Up to 50,000 Feet per Second. NASA TR R-207, 1964.
41. Richardson, Norman R.: Project Fire Instrumentation for Radiative Heating and Related Measurements. NASA TN D-3646, 1966.

TABLE I.- FIRE II PARAMETERS AND SUMMARY OF CALCULATED VALUES

(1) t, sec	(2) $\Delta t$ , sec	(3) h,		(4) $V_{\infty}$ ,		(5) $\rho_{\infty}/\rho_0$	(6) $\rho_{\infty}/\rho_{atd}$	(7) $\text{Log } \rho_2/\rho_{ref}$	(8) $\text{Log } p_2/p_{ref}$	(9) $\rho_2/\rho_{\infty}$	(10) $T_2$ , °K	(11) $\delta_{ne}$ , cm	(12) $d_{0.1}$ , cm	(13) $\delta_{ne} - d_{0.1}$ , cm	(14) $d_p$ , cm
		km	feet	km/sec	fps										
1626.0	8.25	98.46	323060	11.37	37301	0.9038E-06	0.8677E-06					5.76	70.98	TRUNC	33.24
1627.0	9.25	95.67	313891	11.37	37307	0.1393E-05	0.1334E-05					5.30	49.41	TRUNC	22.62
1628.0	10.25	92.89	304757	11.37	37313	0.2242E-05	0.2152E-05					4.90	33.06	TRUNC	14.76
1629.0	11.25	90.11	295659	11.37	37316	0.3413E-05	0.3277E-05					4.64	23.22	TRUNC	10.14
1630.0	12.25	87.35	286598	11.37	37317	0.5020E-05	0.4819E-05					4.46	16.79	TRUNC	7.18
1631.0	13.25	84.60	277574	11.37	37315	0.7770E-05	0.7459E-05					4.32	11.63	TRUNC	4.86
1632.0	14.25	81.86	268588	11.37	37307	0.1215E-04	0.1166E-04					4.23	7.99	TRUNC	3.26
1633.0	15.25	79.13	259640	11.37	37291	0.1873E-04	0.1798E-04					4.19	5.55	TRUNC	2.21
1634.0	16.25	76.42	250735	11.36	37261	0.3160E-04	0.3034E-04	-3.301	-1.351	17.40	10430	4.16	3.57	0.59	1.39
1635.0	17.25	73.72	241878	11.36	37206	0.5076E-04	0.4873E-04	-3.102	-1.147	17.15	10699	4.17	2.40	1.77	0.91
1636.0	18.25	71.04	233074	11.31	37119	0.7272E-04	0.6981E-04	-2.950	-0.993	16.96	10910	4.19	1.77	2.42	0.66
1637.0	19.25	68.37	224330	11.28	36994	0.1046E-03	0.1004E-03	-2.797	-0.839	16.77	11101	4.22	1.30	2.92	0.48
1638.0	20.25	65.73	215659	11.22	36814	0.1454E-03	0.1396E-03	-2.662	-0.700	16.48	11185	4.29	0.99	3.30	0.35
1639.0	21.25	63.11	207072	11.14	36564	0.2045E-03	0.1963E-03	-2.522	-0.559	16.16	11262	4.36	0.74	3.62	0.26
1640.0	22.25	60.53	198589	11.04	36218	0.2824E-03	0.2711E-03	-2.390	-0.427	15.86	11314	4.44	0.57	3.87	0.20
1641.0	23.25	57.98	190234	10.90	35754	0.3809E-03	0.3657E-03	-2.266	-0.309	15.67	11326	4.49	0.44	4.05	0.15
1642.0	24.25	55.48	182033	10.71	35149	0.5074E-03	0.4871E-03	-2.147	-0.199	15.45	11232	4.55	0.35	4.20	0.12
1643.0	25.25	53.04	174020	10.48	34377	0.6624E-03	0.6359E-03	-2.032	-0.103	15.45	11232	3.92	0.35	3.57	0.12
1644.0	26.25	50.67	166232	10.19	33422	0.8622E-03	0.8277E-03	-1.920	-0.013	15.33	10721	3.95	0.22	3.73	0.09
1645.0	27.25	48.37	158713	9.83	32254	0.1120E-02	0.1075E-02	-1.807	0.070	15.33	10138	3.95	0.18	3.77	0.06
1646.0	28.25	46.18	151506	9.41	30861	0.1473E-02	0.1414E-02	-1.680	0.151	15.60	9306	3.88	0.14	3.74	0.05
1647.0	29.25	44.09	144665	8.90	29186	0.1934E-02	0.1857E-02	-1.550	0.221	16.02	8499	3.78	0.11	3.67	0.04
1648.0	30.25	42.14	138247	8.30	27241	0.2543E-02	0.2441E-02	-1.434	0.280	15.93	7923	3.80	0.09	3.71	0.03
1648.0	30.25	42.14	138247	8.30	27241	0.2543E-02	0.2441E-02	-1.434	0.280	15.93	7923	3.31	0.09	3.22	0.03
1649.0	31.25	40.33	132308	7.63	25037	0.3329E-02	0.3196E-02	-1.333	0.323	15.35	7514	3.44	0.07	3.37	0.02
1650.0	32.25	38.67	126890	6.91	22681	0.4205E-02	0.4037E-02	-1.259	0.337	14.42	7121	3.66	0.06	3.60	0.02
1651.0	33.25	37.19	122008	6.19	20313	0.5139E-02	0.4934E-02	-1.211	0.326	13.17	6694	4.01	0.05	3.96	0.01
1652.0	34.25	35.86	117645	5.49	18021	0.6181E-02	0.5934E-02	-1.174	0.299	11.92	6222	4.44	0.04	4.40	0.01

Note: Each tabulated decimal value followed by a whole number indicates the power of 10 by which the decimal value is to be multiplied.

TABLE I.- FIRE II PARAMETERS AND SUMMARY OF CALCULATED VALUES - Continued

(1) t, sec	(15) F <sub>cl</sub>	(16) q <sub>ne'</sub> (ref. 18) W/cm <sup>2</sup>	(17) q <sub>mc'</sub> (ref. 7) (0.23μ < λ < 2.0μ) W/cm <sup>2</sup>	(18) q <sub>mc'</sub> (ref. 6) (0.2μ < λ < 10μ) W/cm <sup>2</sup>	(19) q <sub>mc'</sub> (ref. 8) (0.2μ < λ < 10μ) W/cm <sup>2</sup>	(20) q <sub>mc'</sub> (ref. 11) (λ > 0.2μ) W/cm <sup>2</sup>	(21) q <sub>al'</sub> (ref. 11) (λ > 0.2μ) W/cm <sup>2</sup>	(22) q <sub>al'</sub> (ref. 11) (λ < 0.2μ) W/cm <sup>2</sup>	(23) q <sub>cont'</sub> (ref. 11) (λ < 0.2μ) W/cm <sup>2</sup>
1626.0	0.000	0.2	TRUNC	TRUNC	TRUNC	TRUNC	TRUNC	TRUNC	TRUNC
1627.0	0.000	0.4	TRUNC	TRUNC	TRUNC	TRUNC	TRUNC	TRUNC	TRUNC
1628.0	0.000	0.8	TRUNC	TRUNC	TRUNC	TRUNC	TRUNC	TRUNC	TRUNC
1629.0	0.000	1.4	TRUNC	TRUNC	TRUNC	TRUNC	TRUNC	TRUNC	TRUNC
1630.0	0.000	2.5	TRUNC	TRUNC	TRUNC	TRUNC	TRUNC	TRUNC	TRUNC
1631.0	0.004	5.0	TRUNC	TRUNC	TRUNC	TRUNC	TRUNC	TRUNC	TRUNC
1632.0	0.088	9.5	TRUNC	TRUNC	TRUNC	TRUNC	TRUNC	TRUNC	TRUNC
1633.0	0.278	13.6	TRUNC	TRUNC	TRUNC	TRUNC	TRUNC	TRUNC	TRUNC
1634.0	0.627	15.1	0.3	1.4	0.7	0.6	1.4	3.8	2.2
1635.0	0.871	15.0	2.0	11.2	4.7	4.5	8.7	18.3	13.5
1636.0	0.972	14.9	5.8	31.7	12.2	12.0	21.8	38.4	31.6
1637.0	1.000	14.7	13.9	69.3	28.6	26.6	45.6	67.8	55.6
1638.0	1.000	14.4	25.8	119.0	52.7	46.4	77.4	100.0	77.8
1639.0	1.000	14.0	46.3	201.0	95.2	79.9	129.0	148.0	105.0
1640.0	1.000	13.5	76.7	316.0	160.0	128.0	203.0	207.0	134.0
1641.0	1.000	12.8	116.0	460.0	245.0	188.0	295.0	272.0	158.0
1642.0	1.000	12.0	150.0	588.0	330.0	235.0	385.0	307.0	162.0
1643.0	1.000	12.0	128.0	500.0	281.0	202.0	326.0	284.0	146.0
1644.0	1.000	11.0	146.0	558.0	330.0	214.0	380.0	274.0	131.0
1645.0	1.000	9.9	147.0	523.0	306.0	180.0	341.0	235.0	96.6
1646.0	1.000	8.6	115.0	359.0	198.0	105.0	213.0	144.0	48.5
1647.0	1.000	7.2	74.4	178.0	94.0	56.2	75.4	46.7	12.2
1648.0	1.000	5.8	49.3	90.6	44.9	49.0	21.8	12.1	2.3
1649.0	1.000	4.4	38.0	61.3	29.4	54.0	8.4	4.2	0.6
1648.0	1.000	4.4	33.0	53.3	25.6	46.9	7.4	3.8	0.5
1649.0	1.000	3.2	25.1	43.4	20.6	55.3	3.4	1.5	0.2
1650.0	1.000	2.2	18.4	33.8	16.2	46.5	1.6	0.6	0.0
1651.0	1.000	1.4	14.1	22.5	11.0	36.0	0.5	0.1	0.0
1652.0	1.000	0.9	9.6	13.3	6.7	22.8	0.1	0.0	0.0

TABLE I.- FIRE II PARAMETERS AND SUMMARY OF CALCULATED VALUES - Continued

(1) t, sec	(24) $\dot{q}_e,$ (20) + (21) + (22) + (23) W/cm <sup>2</sup>	(25) $\dot{q}_e,$ (ref. 10) W/cm <sup>2</sup>	(26) $\dot{q}_t,$ (15) × ((16) + (24)) W/cm <sup>2</sup>	(27) $\dot{q}_t,$ (15) × ((16) + (25)) W/cm <sup>2</sup>	(28) $\dot{q}_t,$ (ref. 11) (λ > 0.2μ) W/cm <sup>2</sup>	(29) $\dot{q}_t,$ (ref. 10) (λ > 0.2μ) W/cm <sup>2</sup>	(30) E, $\left( \frac{1}{2} \rho_{\infty} V_{\infty}^3 \right)$ W/cm <sup>2</sup>	(31) $\dot{q}_c,$ (ref. 39) W/cm <sup>2</sup>
1625.0	TRUNC	TRUNC	0.0	0.0	0.0	0.0	78	0.0
1627.0	TRUNC	TRUNC	0.0	0.0	0.0	0.0	120	37.6
1628.0	TRUNC	TRUNC	0.0	0.0	0.0	0.0	194	45.0
1629.0	TRUNC	TRUNC	0.0	0.0	0.0	0.0	295	55.6
1630.0	TRUNC	TRUNC	0.0	0.0	0.0	0.0	434	68.8
1631.0	TRUNC	TRUNC	0.0	0.0	0.0	0.0	672	88.6
1632.0	TRUNC	TRUNC	0.8	0.8	0.8	0.8	1050	109.0
1633.0	TRUNC	TRUNC	3.8	3.8	3.8	3.8	1617	134.0
1634.0	8.0	*	14.5	0.0	10.5	0.0	2722	172.0
1635.0	45.0	41.8	52.2	49.5	23.1	22.4	4353	220.0
1636.0	104.0	77.6	116.0	90.0	42.1	35.1	6192	268.0
1637.0	195.0	137.0	210.0	152.0	75.3	57.3	8817	312.0
1638.0	301.0	211.0	315.0	225.0	118.0	86.4	12080	357.0
1639.0	462.0	320.0	476.0	334.0	189.0	135.0	16640	407.0
1640.0	672.0	461.0	685.0	474.0	292.0	204.0	22340	458.0
1641.0	913.0	620.0	926.0	633.0	419.0	288.0	28990	511.0
1642.0	1099.0	764.0	1101.0	776.0	533.0	378.0	36690	561.0
1642.0	958.0	692.0	970.0	704.0	455.0	332.0	36690	645.0
1643.0	999.0	768.0	1010.0	779.0	510.0	395.0	44810	678.0
1644.0	953.0	782.0	863.0	792.0	448.0	411.0	53590	685.0
1645.0	510.0	*	519.0	*	276.0	*	62570	674.0
1646.0	190.0	*	197.0	*	118.0	*	72090	665.0
1647.0	85.0	*	90.8	*	65.3	*	80060	632.0
1648.0	67.1	*	71.5	*	56.8	*	85590	578.0
1648.0	58.6	*	63.0	*	50.0	*	85590	675.0
1649.0	60.4	*	63.6	*	52.5	*	86990	578.0
1650.0	48.7	*	50.9	*	42.6	*	81690	466.0
1651.0	36.6	*	38.0	*	32.0	*	71720	258.0
1652.0	22.9	*	23.8	*	20.1	*	60230	353.0

\* Flight conditions outside range of theory.

TABLE I.- FIRE II PARAMETERS AND SUMMARY OF CALCULATED VALUES - Concluded

(1) t, sec	(32) $\alpha_{Be}^{(16)}$ ( $\alpha_{Be} = 0.54$ ) W/cm <sup>2</sup>	(33) $\alpha_{Be}^{(20)}$ ( $\alpha_{Be} = 0.54$ ) W/cm <sup>2</sup>	(34) $\alpha_{Be}^{(21)}$ ( $\alpha_{Be} = 0.52$ ) W/cm <sup>2</sup>	(35) $\alpha_{Be}^{(22)}$ ( $\alpha_{Be} = 0.75$ ) W/cm <sup>2</sup>	(36) $\alpha_{Be}^{(23)}$ ( $\alpha_{Be} = 0.94$ ) W/cm <sup>2</sup>	(37) $F_{cl} \sum \alpha_{Be} \dot{q}_r$ (15) × ((32) + (33) + (34) + (35) + (36))	(38) $\dot{q}_c + F_{cl} \sum \alpha_{Be} \dot{q}_r$ (31) + (37)
1626.0	0.1	TRUNC	TRUNC	TRUNC	TRUNC	0.0	0.0
1627.0	0.2	TRUNC	TRUNC	TRUNC	TRUNC	0.0	37.6
1628.0	0.4	TRUNC	TRUNC	TRUNC	TRUNC	0.0	45.0
1629.0	0.8	TRUNC	TRUNC	TRUNC	TRUNC	0.0	55.6
1630.0	1.4	TRUNC	TRUNC	TRUNC	TRUNC	0.0	68.8
1631.0	2.7	TRUNC	TRUNC	TRUNC	TRUNC	0.0	88.6
1632.0	5.1	TRUNC	TRUNC	TRUNC	TRUNC	0.4	109.0
1633.0	7.3	TRUNC	TRUNC	TRUNC	TRUNC	2.0	136.0
1634.0	8.2	0.3	0.7	2.8	2.1	8.8	181.0
1635.0	8.1	2.4	4.5	13.7	12.7	36.5	256.0
1636.0	8.0	6.5	11.3	28.8	29.7	82.6	351.0
1637.0	7.9	14.4	23.8	50.8	52.3	150.0	462.0
1638.0	7.8	25.0	40.2	75.0	73.1	221.0	578.0
1639.0	7.6	43.1	67.0	111.0	98.7	328.0	735.0
1640.0	7.3	69.1	106.0	155.0	126.0	463.0	921.0
1641.0	6.9	102.0	153.0	204.0	149.0	614.0	1125.0
1642.0	6.5	127.0	200.0	230.0	152.0	715.0	1276.0
1642.0	6.5	109.0	170.0	213.0	137.0	636.0	1281.0
1643.0	5.9	116.0	198.0	205.0	123.0	648.0	1326.0
1644.0	5.3	97.3	177.0	176.0	90.8	546.0	1231.0
1645.0	4.6	56.7	111.0	108.0	45.6	326.0	1000.0
1646.0	3.9	30.4	39.2	35.0	11.5	120.0	785.0
1647.0	3.1	26.5	11.3	9.1	2.2	52.4	684.0
1648.0	2.4	29.2	4.4	3.1	0.6	39.7	618.0
1648.0	2.4	25.3	3.9	2.8	0.5	34.9	710.0
1649.0	1.7	29.8	1.8	1.1	0.2	34.6	613.0
1650.0	1.2	25.1	0.9	0.4		27.6	494.0
1651.0	0.8	19.4	0.3	0.1		20.6	374.0
1652.0	0.5	12.3	0.1			12.9	271.0

Beryllium layer	D, m	$r_n$ , m	$r_c$ , m
1	0.672	0.935	0.010
2	.630	.805	.036
3	.587	.702	.006

Sensor locations

- Radiometer
- + Thermocouples
- Δ Static pressure transducer

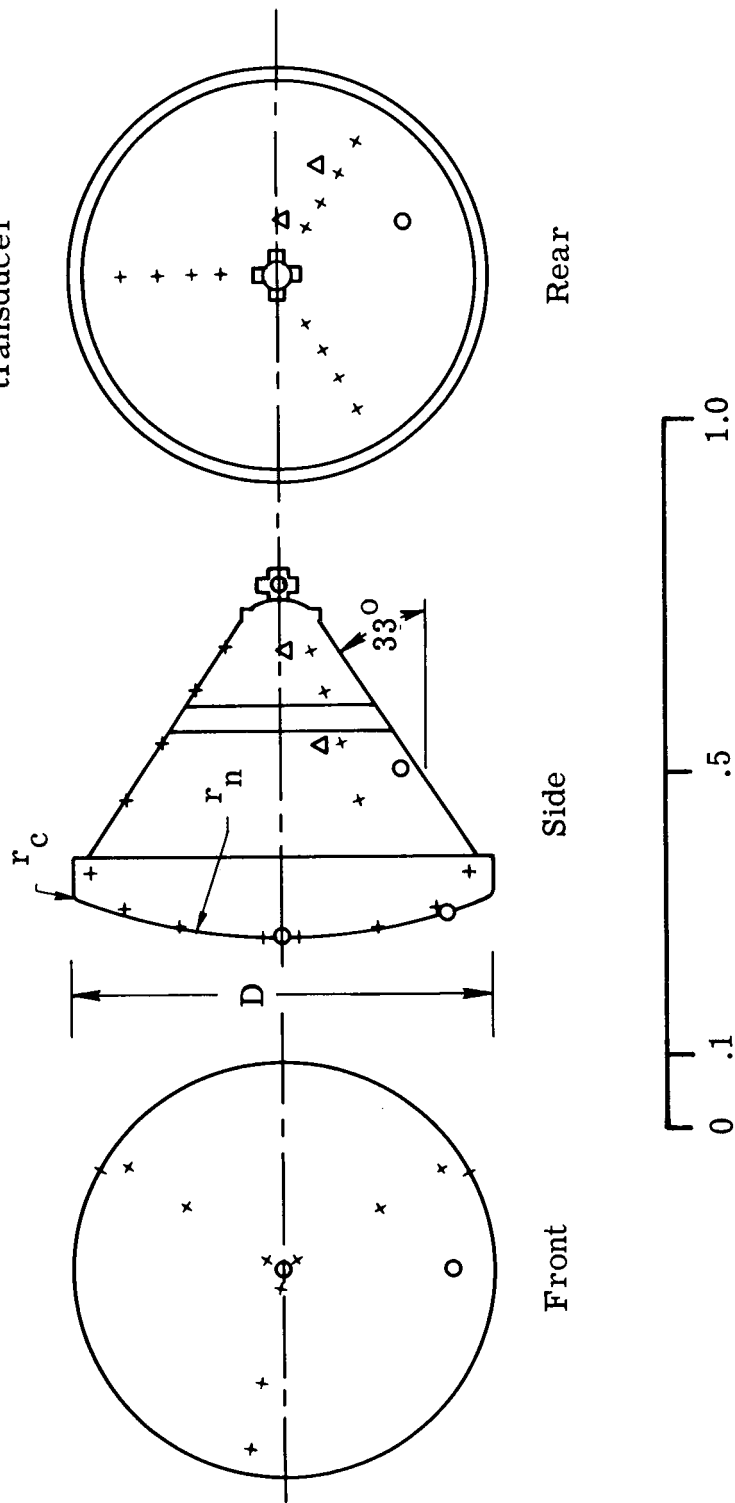


Figure 1.- Reentry package geometry and sensor locations.

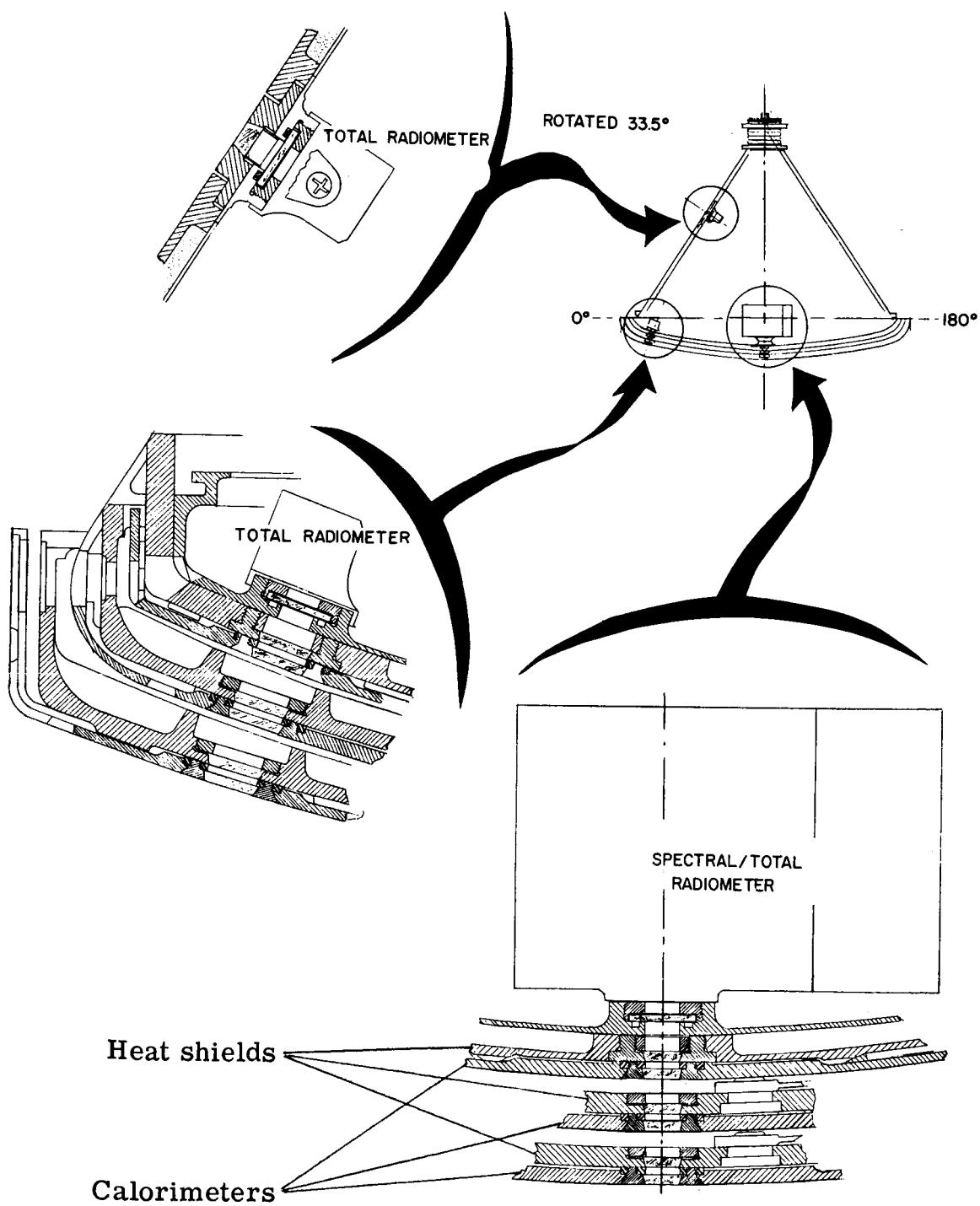


Figure 2.- Location of radiometers and windows.



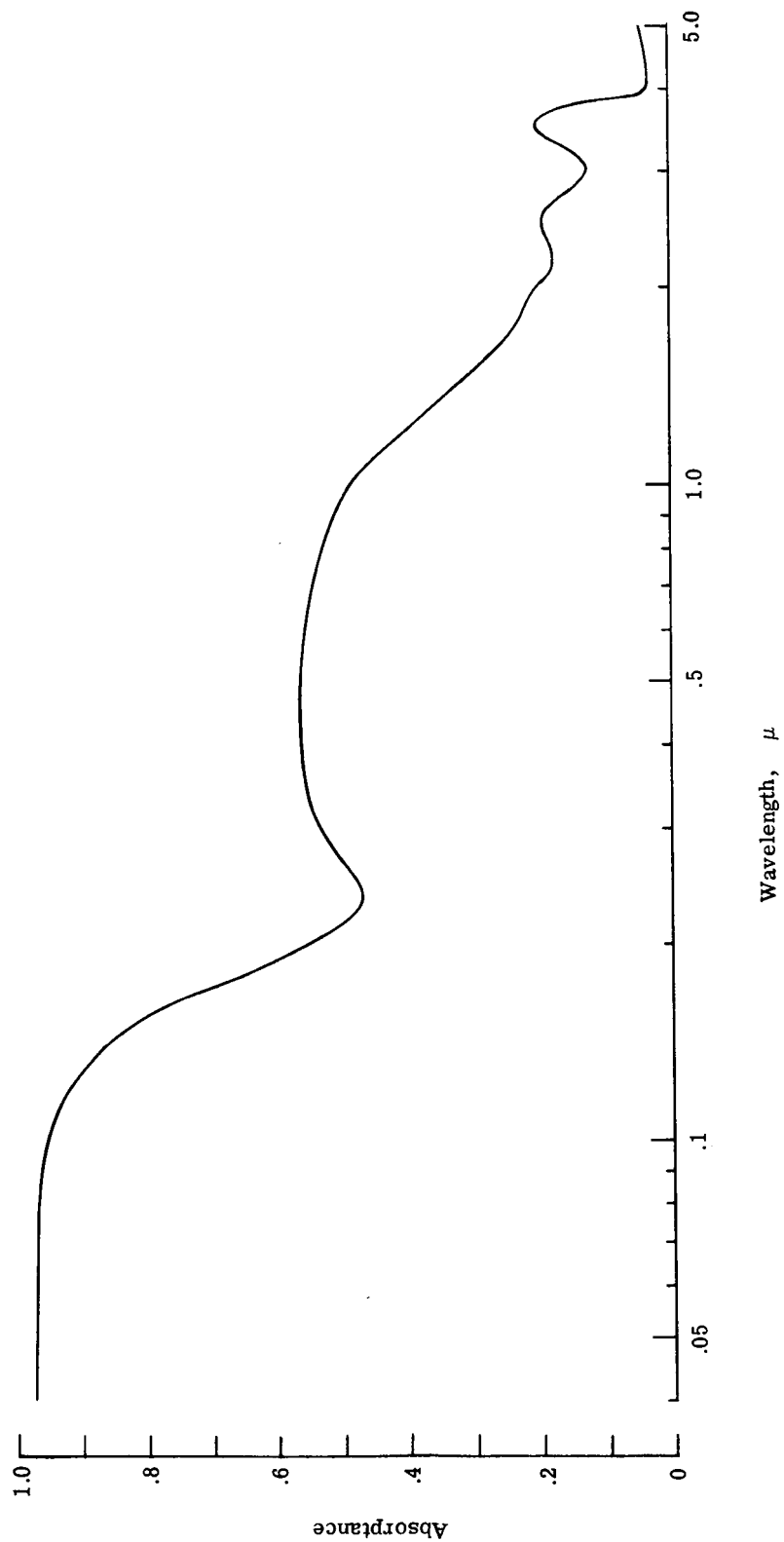
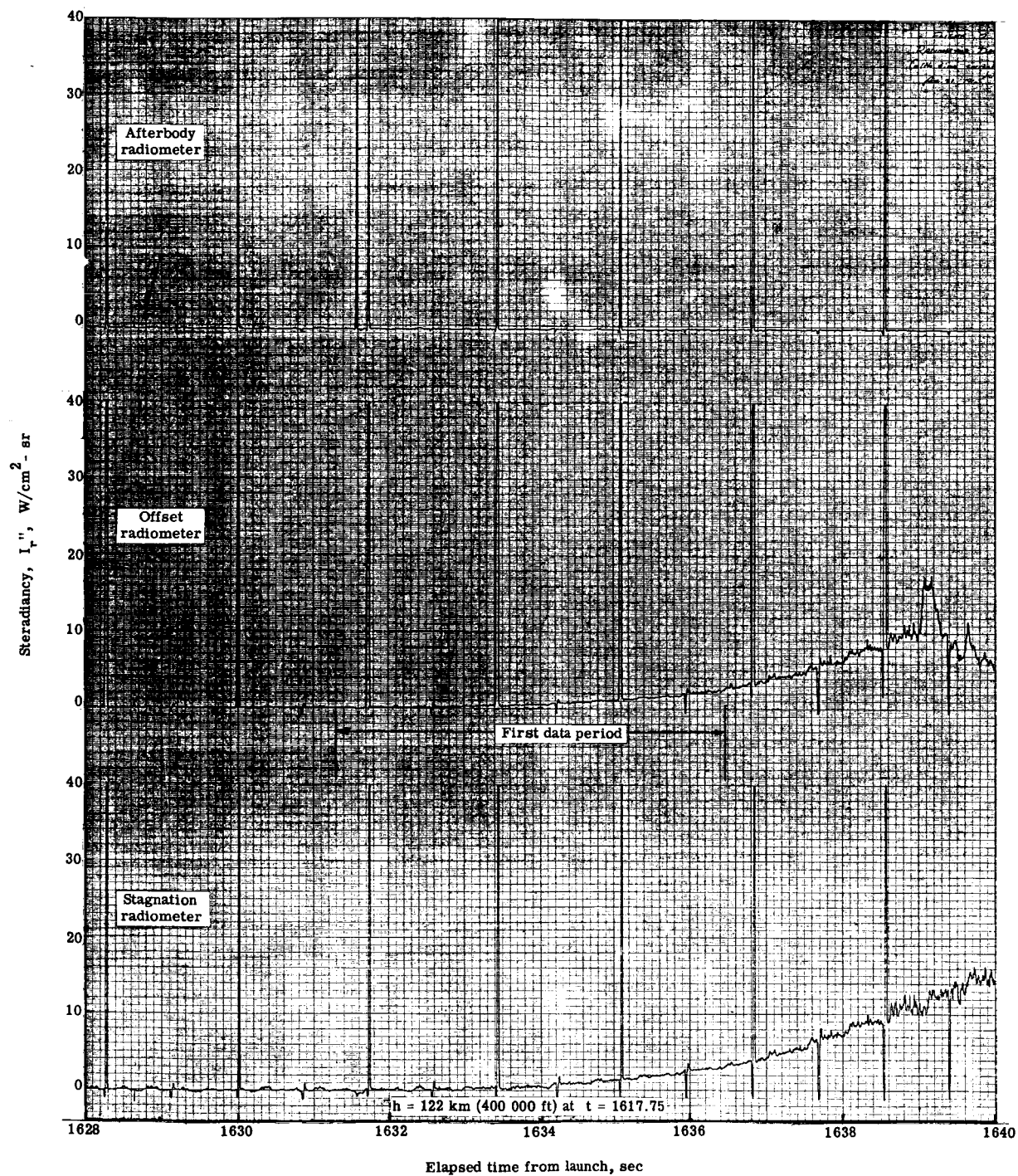
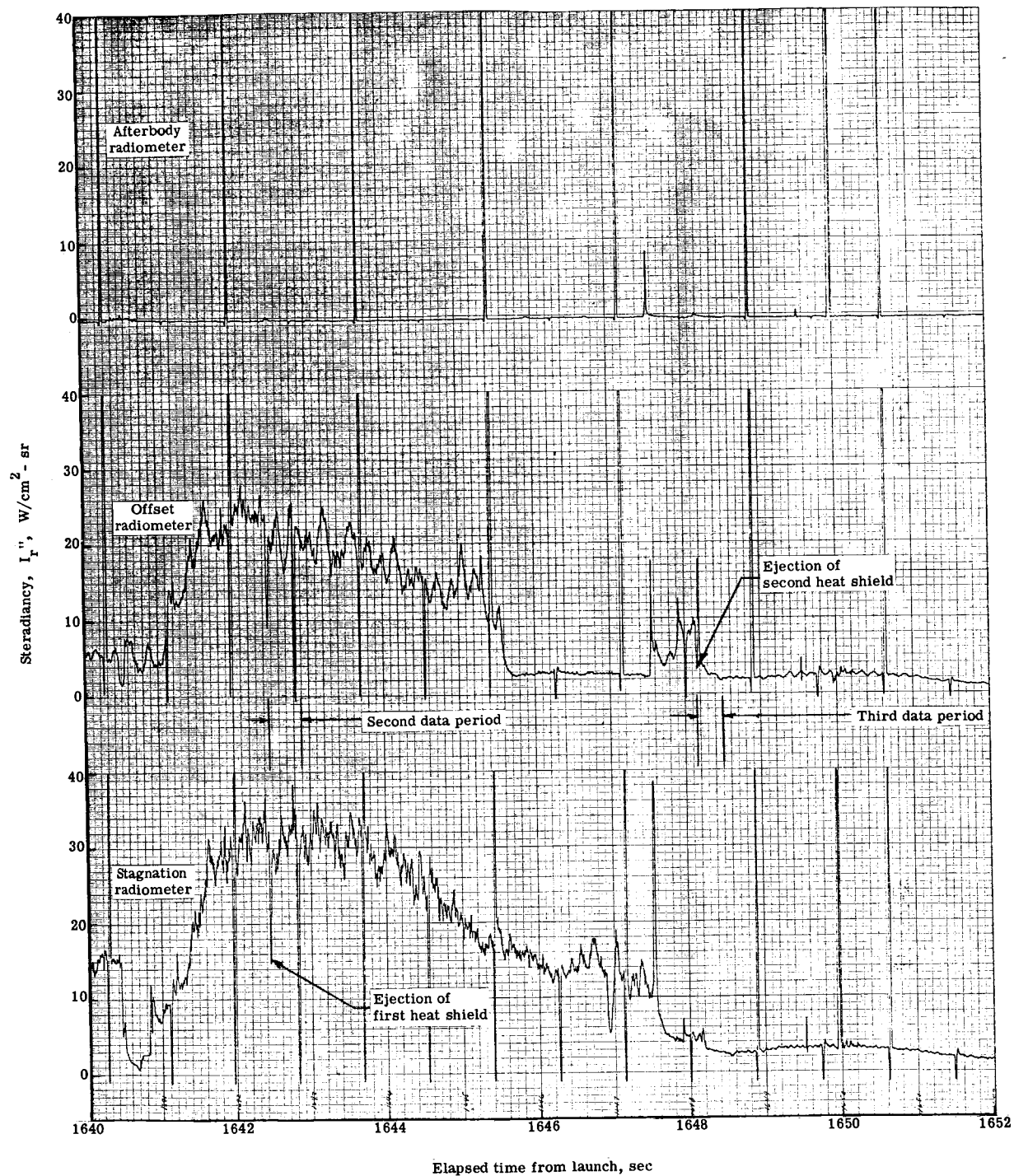


Figure 3.- Spectral absorbance characteristics of polished beryllium at room temperature.



(a) Early reentry.

Figure 4.- Fire II steradiance levels reduced from original telemetry record.



(b) Peak heating and later reentry.

Figure 4.- Concluded.

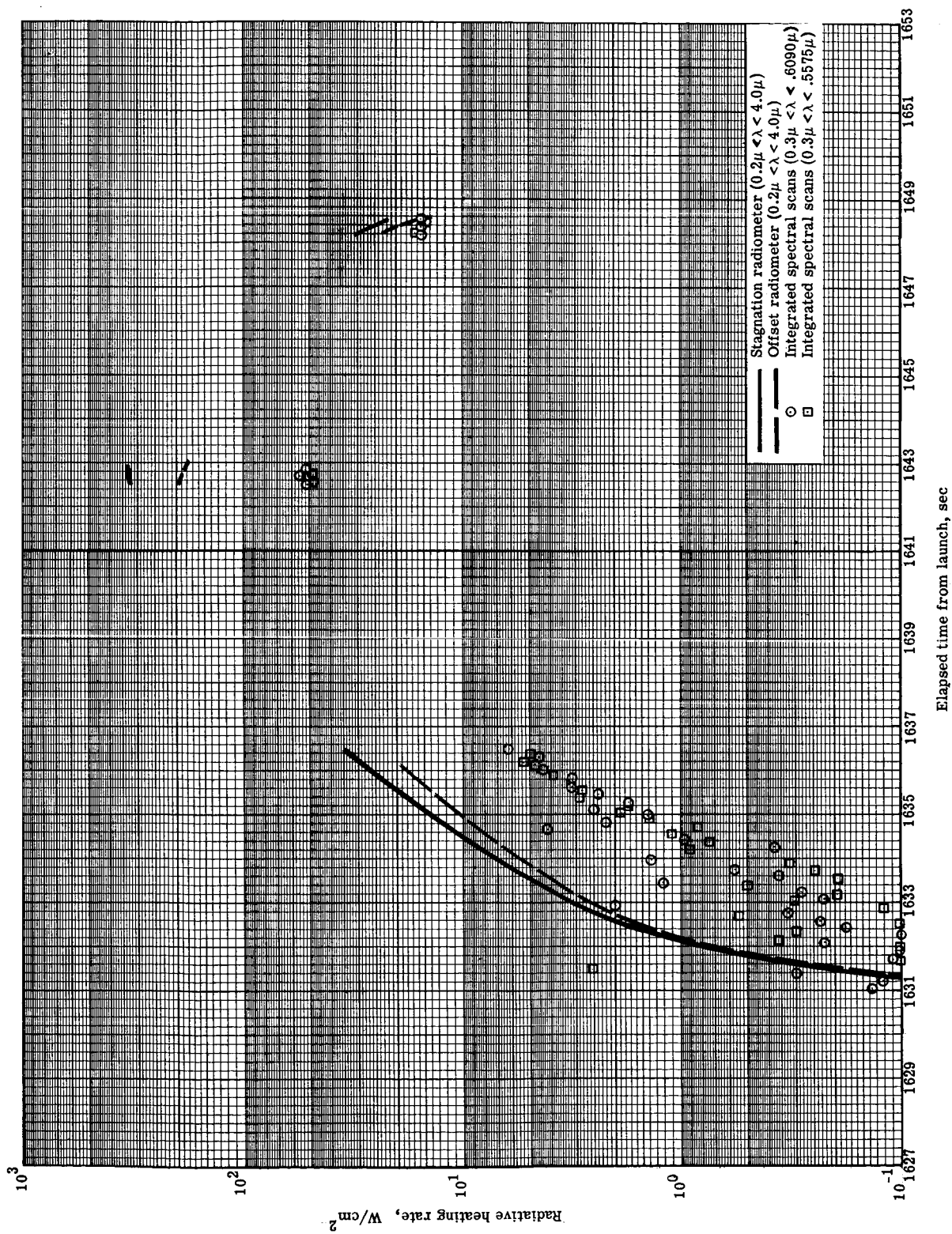


Figure 5.- Fire II experimental forebody heating rates.

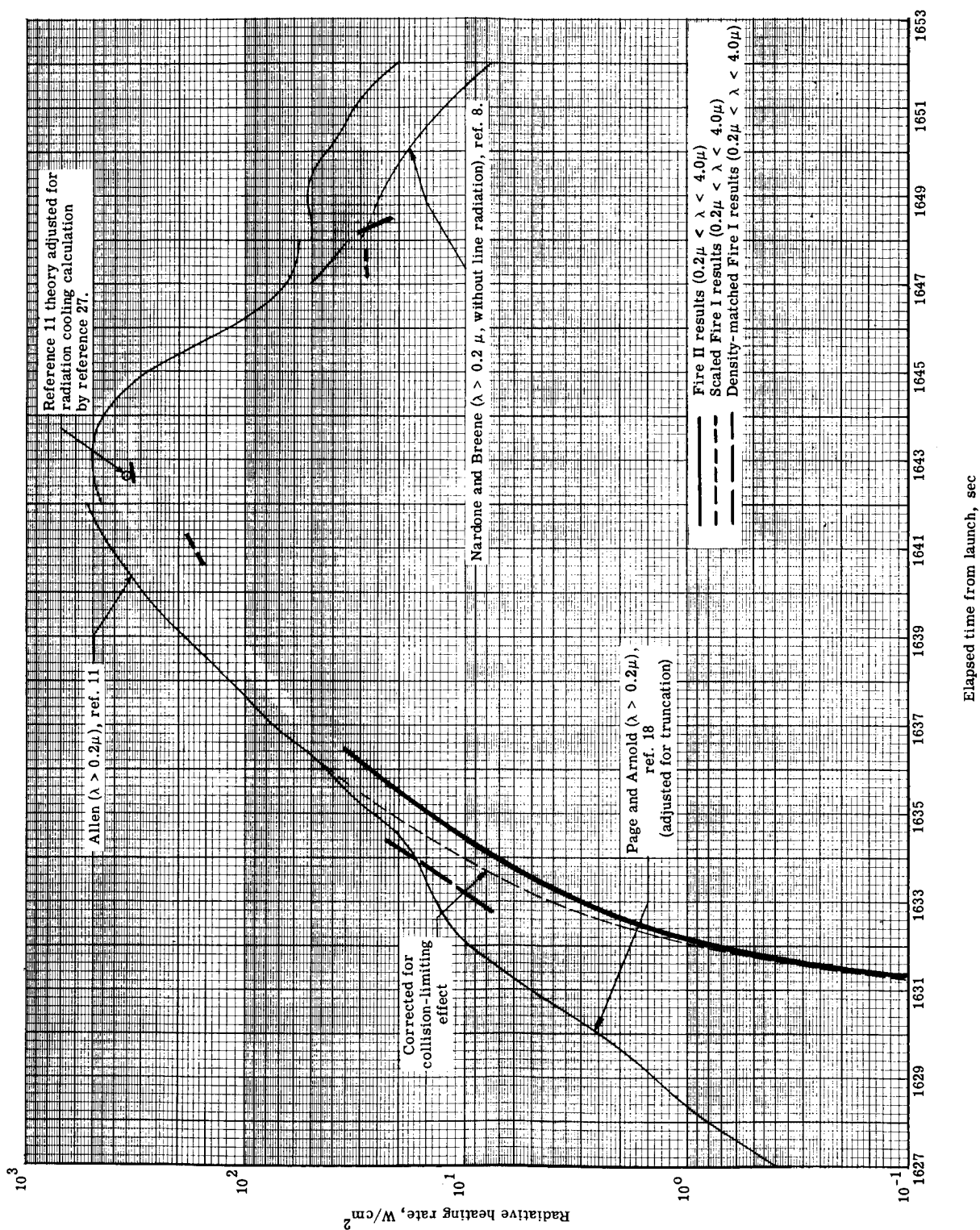


Figure 6.- Comparison of Fire II results with Fire I and theoretical heating rates.

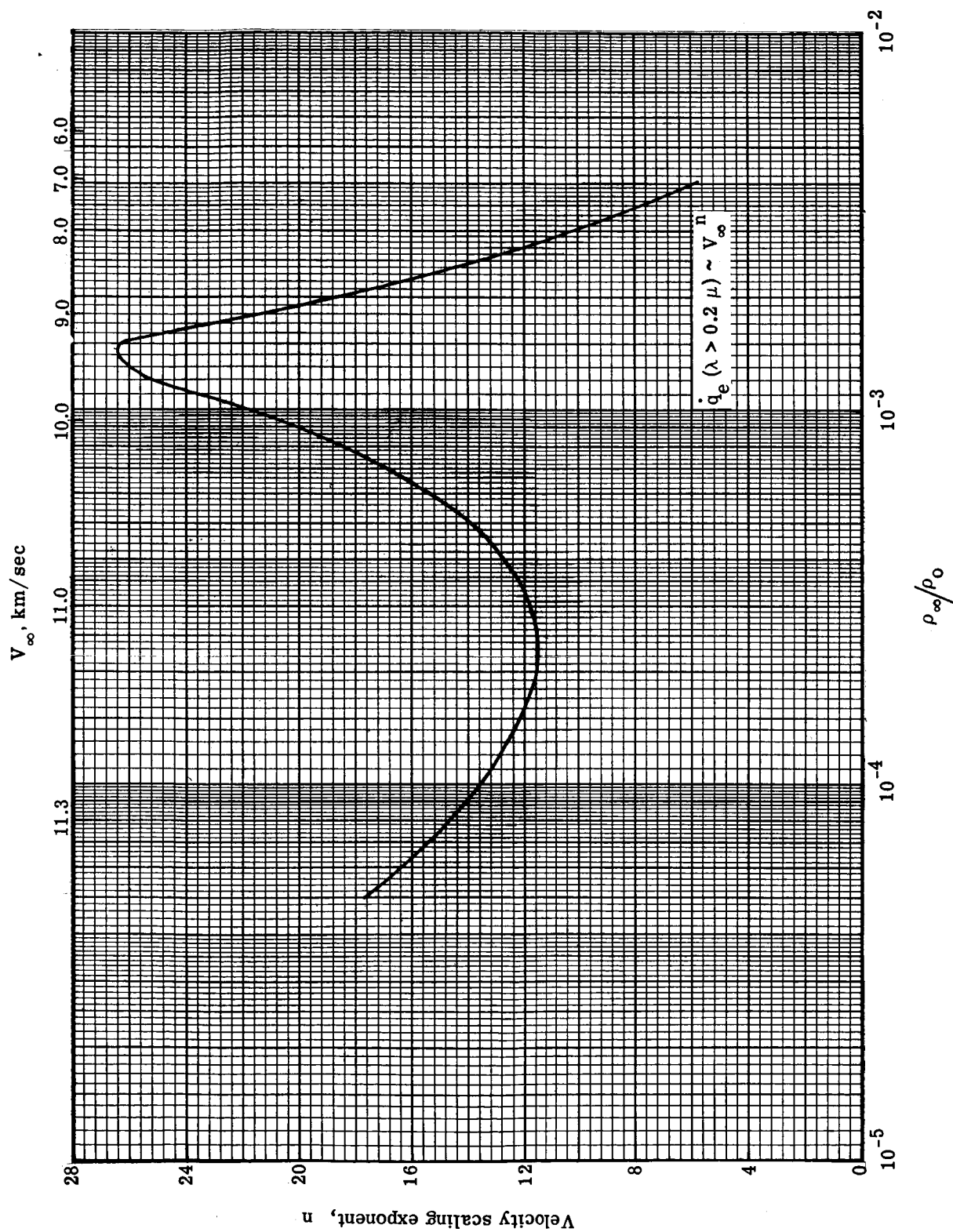


Figure 7.- Velocity dependence of theoretical equilibrium radiation determined from Project Fire reentry trajectories.

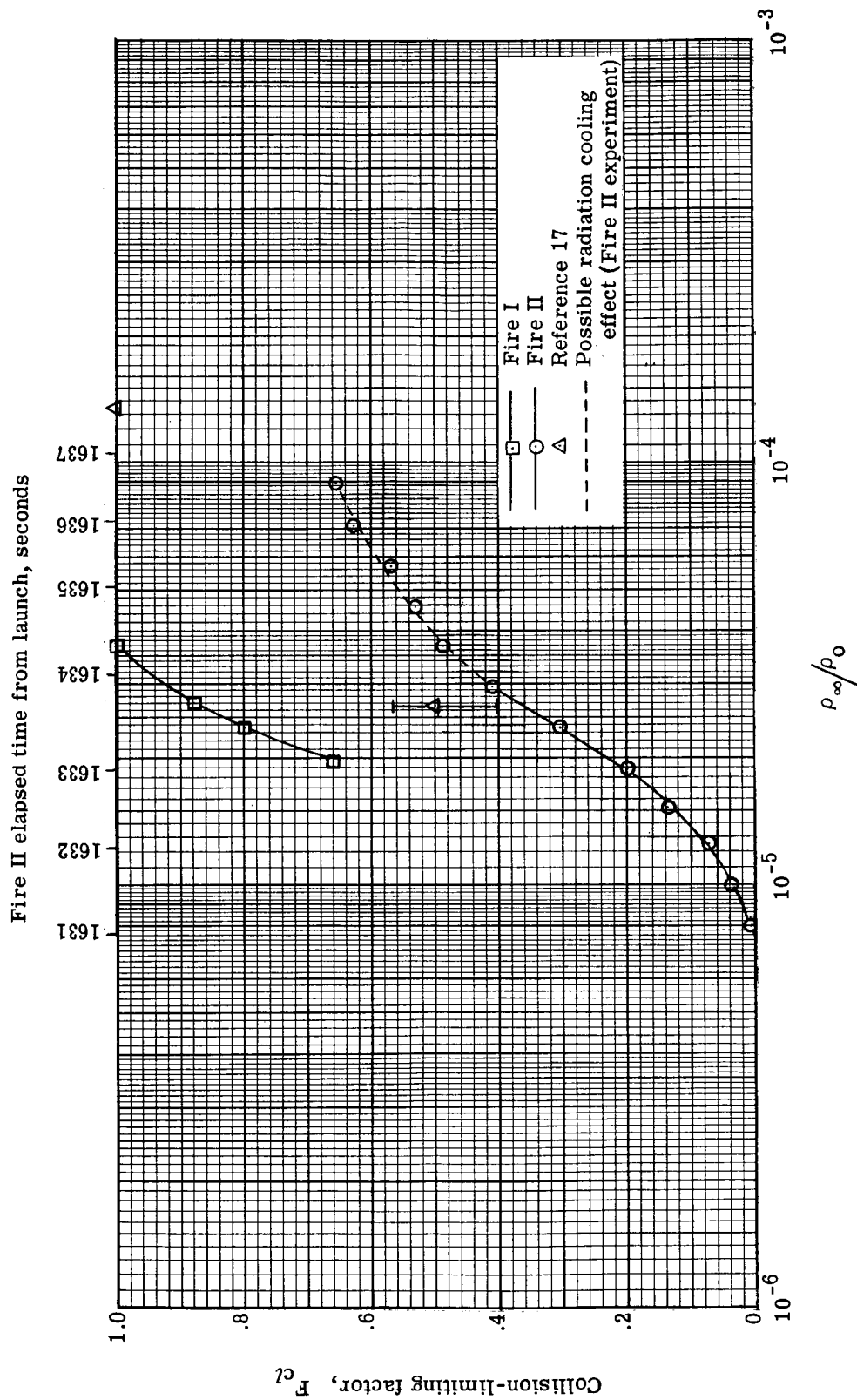


Figure 8.- Collision-limiting data from shock tube and Project Fire reentry experiments.



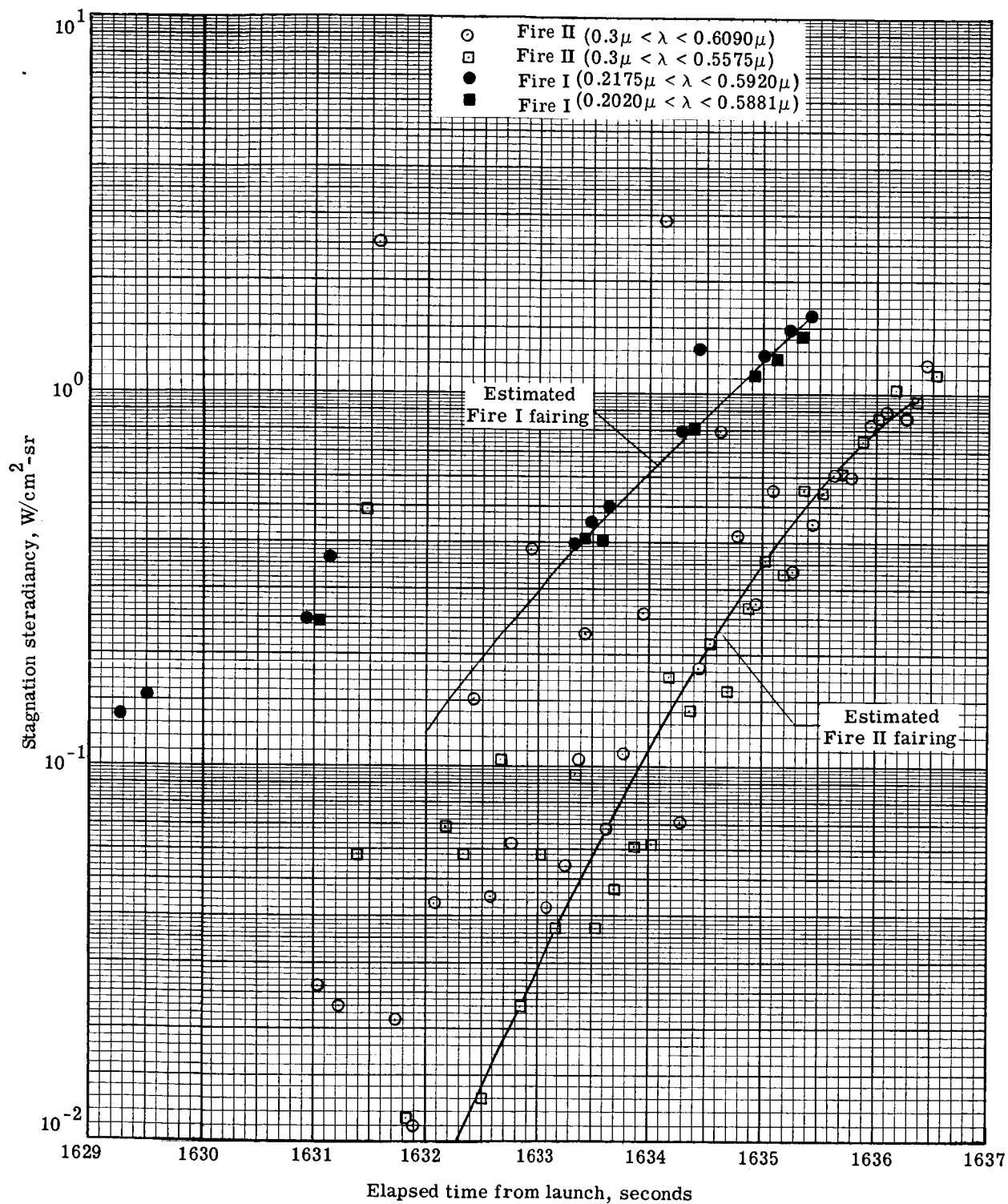


Figure 9.- Stagnation steradiance at surface of Fire reentry package obtained from the integration of the Fire I and Fire II spectral radiometer scans.



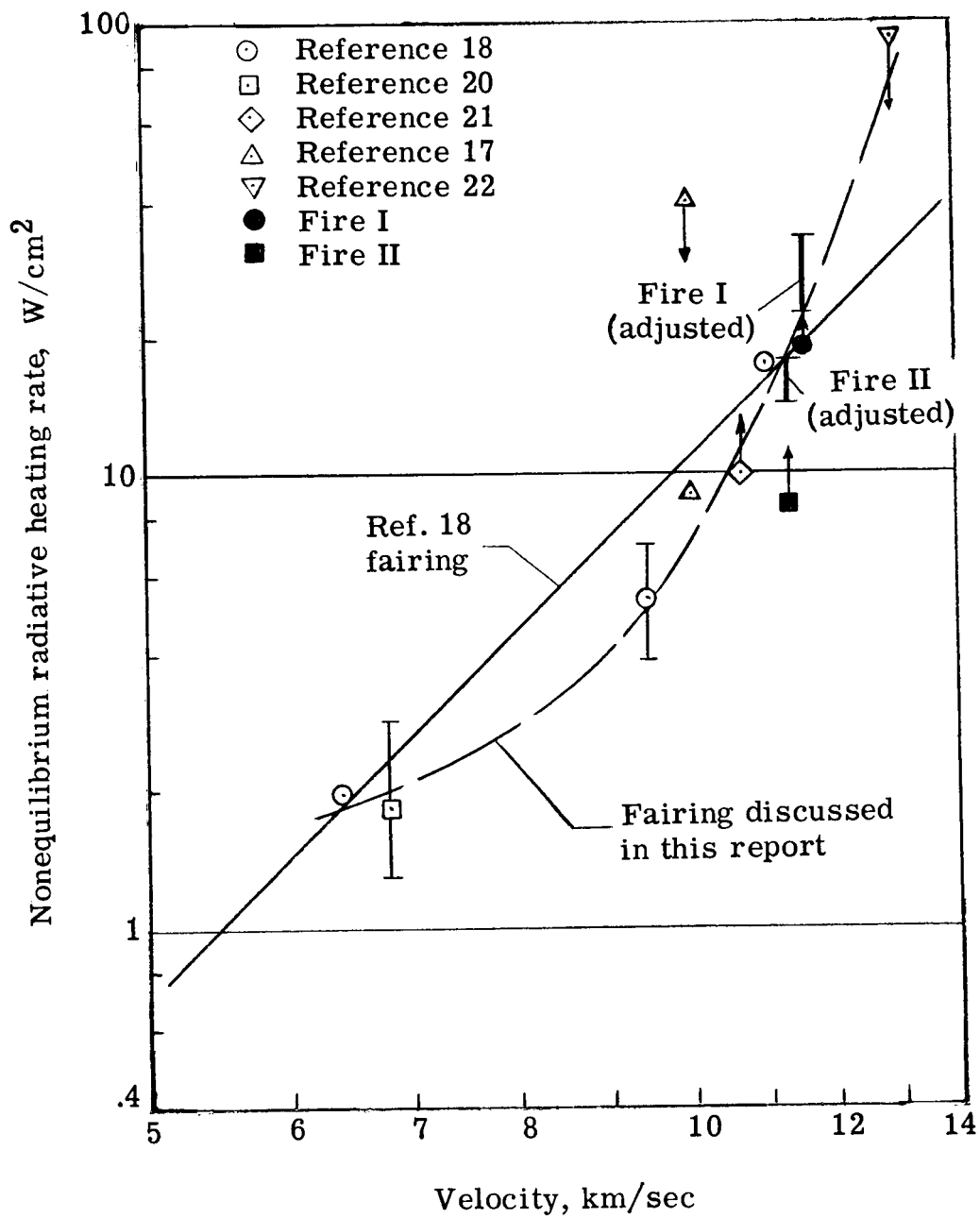


Figure 10.- Summary of Project Fire and ground facility experimental results of nonequilibrium radiative heating.

Fire II elapsed time from launch, seconds

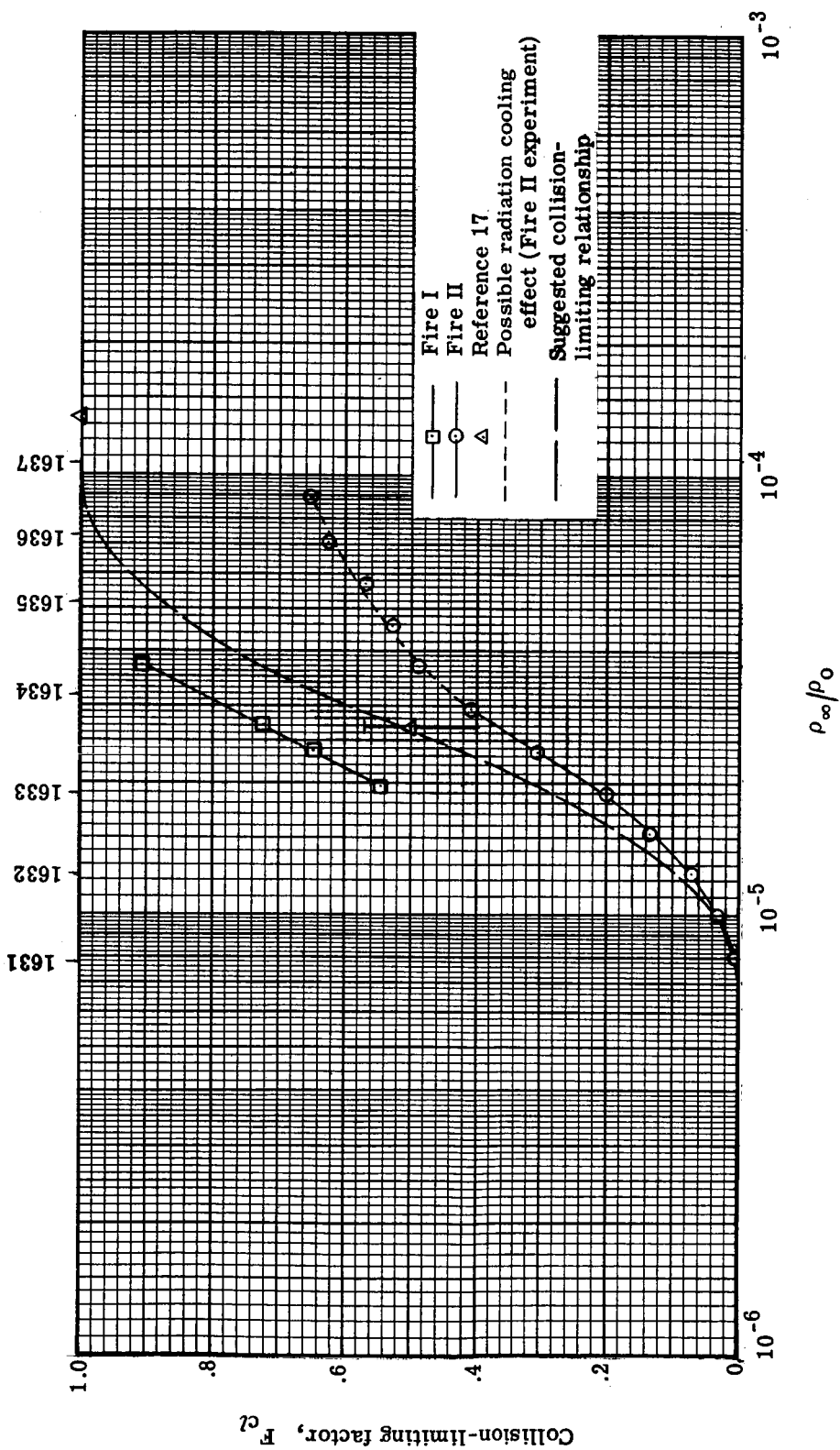


Figure 11.- Collision-limiting estimate based on the Project Fire experimental data and the suggested ninth-power velocity-dependent nonequilibrium radiative heating relationship.

○ □

Theory (refs. 11, 17, 18, and 31 as per text)

Calculations using Fire II integrated spectral radiometer scans ( $0.3\mu < \lambda < 0.6090\mu$ )

Calculations using Fire II integrated spectral radiometer scans ( $0.3\mu < \lambda < 0.5575\mu$ )

$$\text{Percent radiation} = \frac{\text{Total radiometer heating rates, } (0.2\mu < \lambda < 4.0\mu) - \text{Integrated spectral radiometer heating rates, } (0.2\mu < \lambda < 0.3\mu)}{\text{Total radiometer heating rates, } (0.2\mu < \lambda < 4.0\mu)} \times 100$$

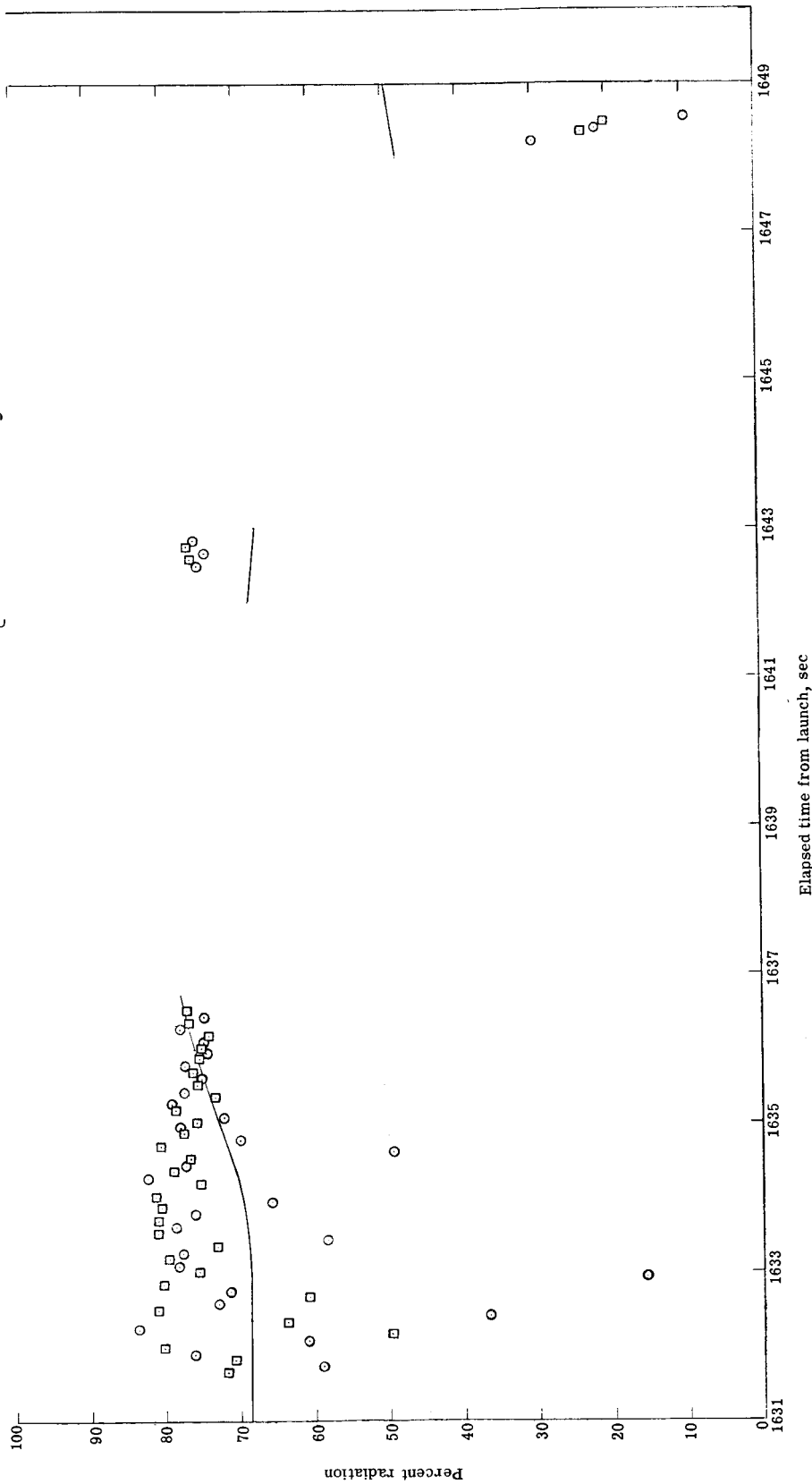


Figure 12.- Percent of stagnation radiative heating at wavelengths longer than  $0.2\mu$  that falls above a nominal wavelength of  $0.6\mu$ .

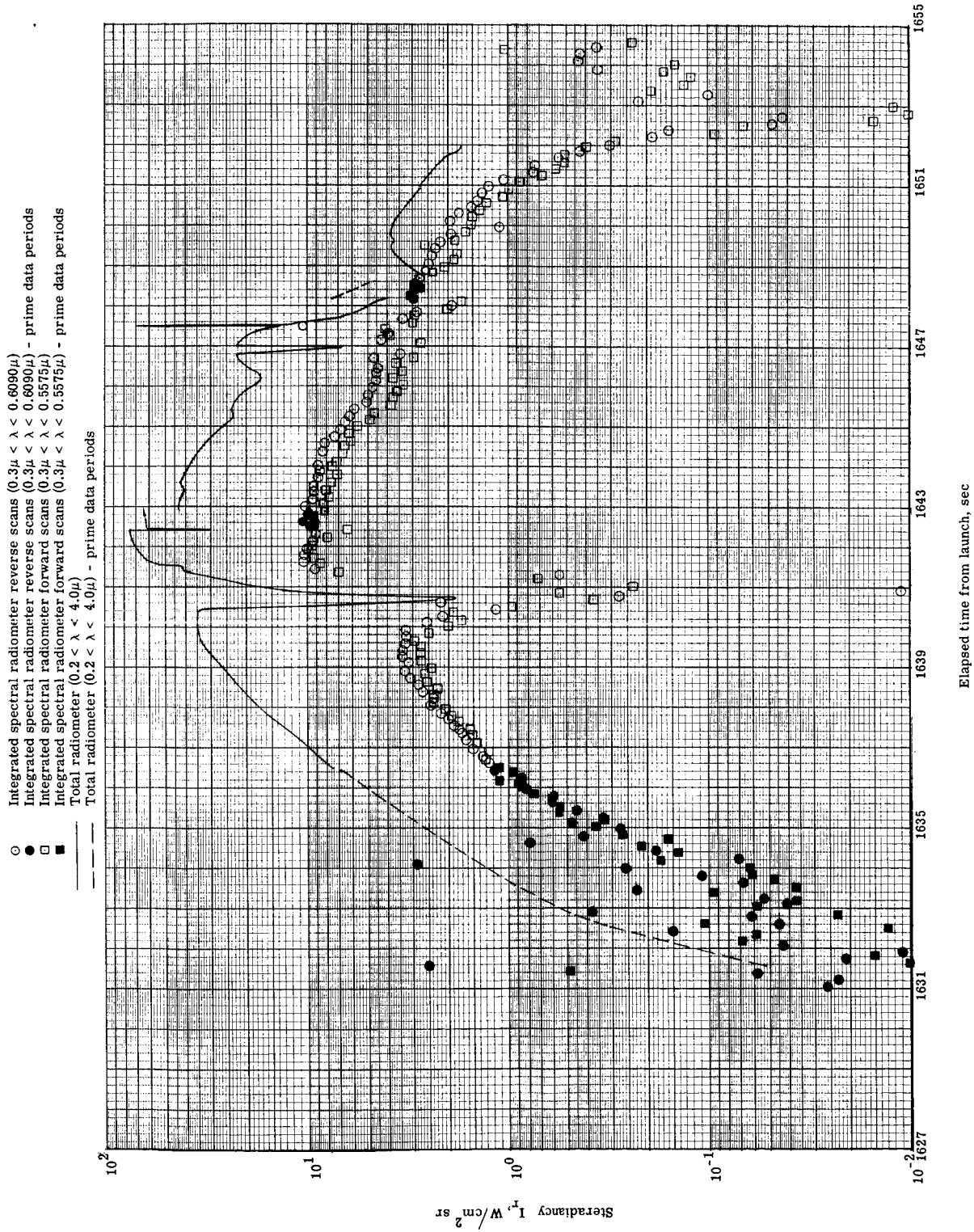


Figure 13.- Reentry time history of steradiance incident at stagnation point of Fire II reentry package.

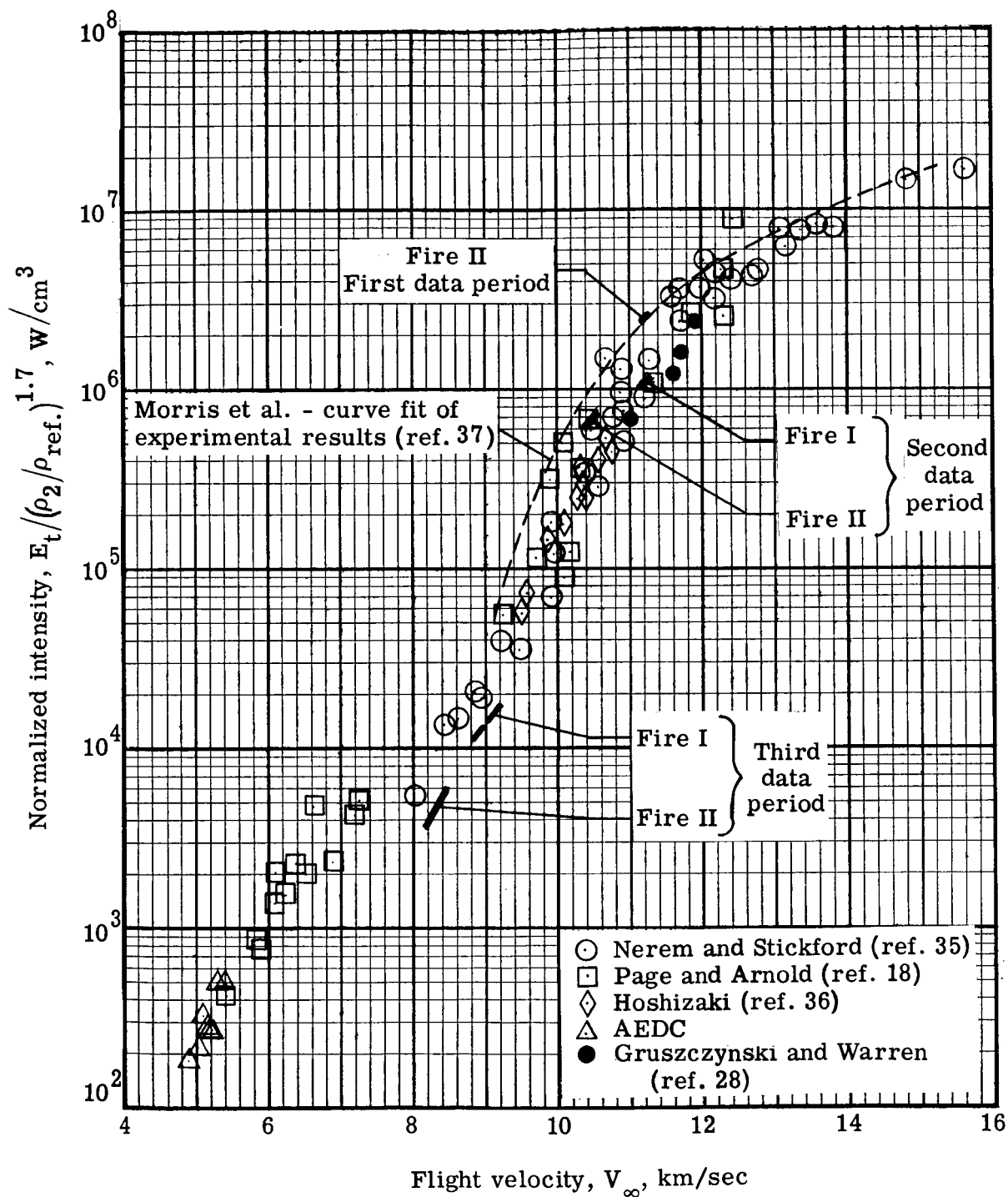


Figure 14.- Comparison of experimental results on stagnation-point equilibrium air radiative emission ( $\lambda > 0.2\mu$ ).

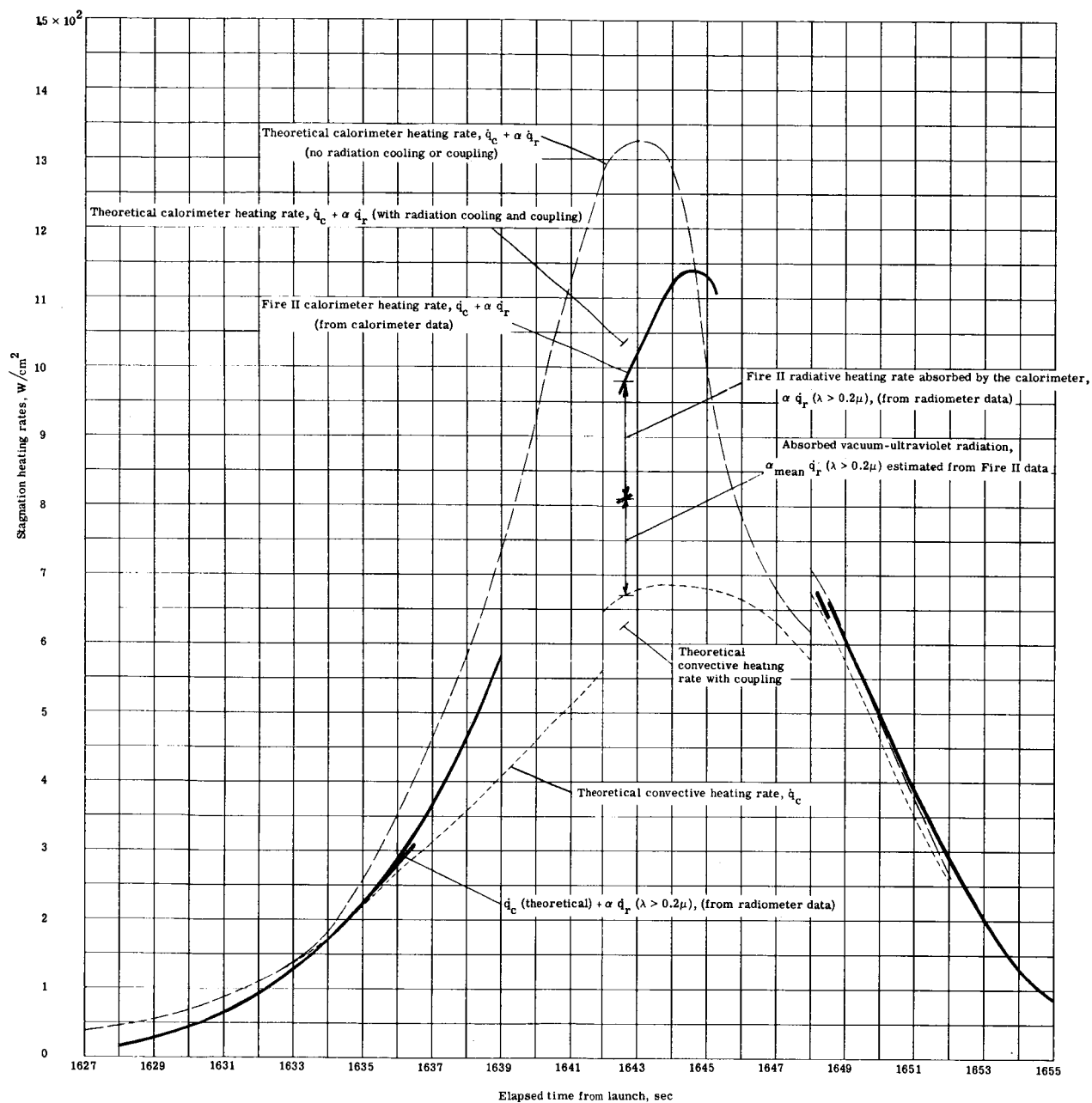


Figure 15.- Method for estimation of vacuum-ultraviolet radiation ( $\lambda < 0.2\mu$ ) from Fire II calorimeter and radiometer experimental results.

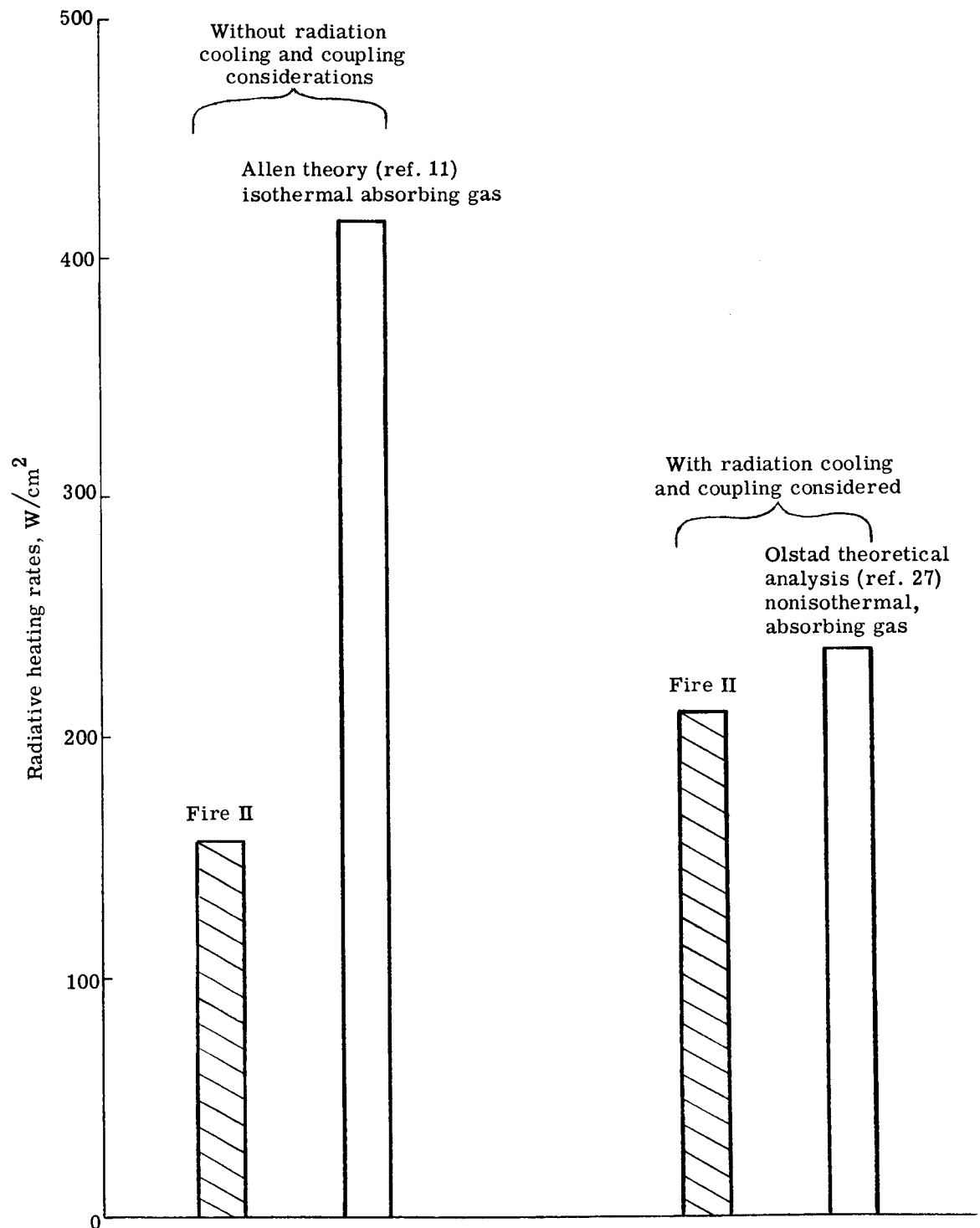


Figure 16.- Comparison of theoretical estimates of vacuum-ultraviolet radiative heating with values deduced from Fire II second data period experiment at  $t = 1642.65$  seconds.